The University of Osaka
Institutional Knowledge Archive

Title	High-Speed Automated Micromanipulation System with Multi-scalability
Author(s)	Avci, Ebubekir
Citation	大阪大学, 2013, 博士論文
Version Type	VoR
URL	https://doi.org/10.18910/26265
rights	
Note	

The University of Osaka Institutional Knowledge Archive : OUKA

https://ir.library.osaka-u.ac.jp/

The University of Osaka

High-Speed Automated Micromanipulation System with Multi-scalability

A dissertation submitted to
THE GRADUATE SCHOOL OF ENGINEERING SCIENCE
OSAKA UNIVERSITY
in partial fulfillment of the requirements for the degree of
DOCTOR OF PHILOSOPHY IN ENGINEERING
BY

EBUBEKIR AVCI

SEPTEMBER 2013

Abstract

High-Speed Automated Micromanipulation System with Multi-scalability

By EBUBEKIR AVCI

Chairperson of the Supervisory Committee: Professor TATSUO ARAI

Numerous types of microhands have recently been designed to perform micromanipulation tasks that are crucial for micromachine assembly, microsurgery operations and biological cell analysis. Because most current microsystems are task-specific, the realization of a general-purpose microhand that is compatible with a wide range of applications is necessary. In addition, to utilize the microhand in complex bioapplications, e.g., 3D cell assembly, stable control at high speed should be achieved.

There are two problems to be solved in order to realize a general-purpose micromanipulation system. First, creating a large workspace with high resolution in which to grasp multisized microobjects is still a challenging feature for available microhands. Second, precise motion throughout a large workspace for the transportation of microobjects in the limited space of a microscope is another arduous task. In this study, we propose multiscalability concept, i.e., a large workspace with precise positioning for the grasping and transportation of multisized microobjects. This system has been designed with an optimized parallel mechanism through inverse kinematics in which the manipulability of different-sized microobjects is improved from 1-45 μm to 1-132 μm. The proposed coarse-to-fine motion strategy that allows us to achieve a large range with high resolution positioning ability for performing the transportation task is moreover minimized from 17 μm error to 0.18 μm.

On the other hand, we present a high-speed pick-and-place method for cell-assembly applications. Besides the range of motion and accuracy, the rapidness of a manipulation system is an important parameter, which has been so far underrated in the literature. To achieve high-speed micromanipulation, obtaining 3D positions of both the target microobject and the end effector rapidly is necessary. Controlling the vibration of the end effector, which is greater at high speed, is another arduous task. We propose a new fast detection algorithm for both the target microobject and the end effector for achieving high-speed control of the system. Moreover, to realize stable grasping for very fast movements, the vibration of the system is compensated. High-speed control of the microhand system is demonstrated with preliminary experiments consisting of pick-and-place actions of 40 to 60 μm microspheres; we aimed at performing a manipulation task in 1 second. The comparison with similar studies shows the merit of the proposed automated high-speed micromanipulation system.

Dedication

To my family

Acknowledgements

Above all, I would like to express my deep and most sincere gratitude to my advisor, Professor Tatsuo ARAI, for his wonderful guidance, and for giving me this great opportunity to be a member of his lab. I could not have been through all my difficult times here without his strong support, caring, patience, and understanding.

I would also like to express my sincere gratitude to Professor Fumio MIYAZAKI and Professor Youji IIGUNI for many invaluable suggestions for the thesis.

I am also truly indebted to Assistant Professor Masaru KOJIMA and Associate Professor Kenichi OHARA, whose encouragement and advice enabled me to develop an understanding of the subject. I am really appreciate their prompt support and guidance. Particularly, I appreciate encouragements of Kojima Sensei when I stuck and lose my passion to continue research.

I would also like to express my gratitude to Assistant Professor Kazuto KAMIYAMA, Assistant Professor Mitsuhiro HORADE, Associate Professor Tomohito TAKUBO and Associate Professor Yasushi MAE, for their guidance and useful discussion during my PhD education.

I am grateful to Amr ALMADDAH and Huseyin UVET for bringing a lot of fun into my life during graduate education and giving me wisdom about doing researches.

I like to thank Puwanan, Ae Kun, Tim, Christian and other lab mates for nice soccer games. I want to thank Kaminade San for his special friendship and Koyama Kun for his valuable helps.

I also acknowledge the financial support from Monbukagakusho for giving me the scholarship to pursue the PhD program at Osaka University, Osaka, Japan.

Last but not least, I like to express my sincere gratitude to my loved one for supporting me in so many different ways and bringing joy into my life.

Contents

1 Introduction 1

1.1 General Background 1

1.1.1 Manipulation in Macro and Micro Scales 2

1.1.2 Micromanipulation Methods 4

1.2 Statement of the Problem 7

1.2.1 Multi-Scalability 7

1.2.2 Micromanipulation at High Speed 9

1.3 Main Contributions 12

1.3.1 Concept of Multi-Scalability 12

1.3.2 Successful Control of Microhand at High Speed 13

1.4 Organization of the Thesis 15

2 Workspace Optimization for Manipulation of Multi-sized Microobjects 17

2.1 System Concept 17

2.2 Workspace Analysis 19

2.3 Workspace Optimization 24

3 Coarse to Fine Manipulation Strategy and Experimental Results 31

3.1 System Construction 31

3.1.1 System Configuration 31

3.1.2 Realization of Multi-Scalability 34

3.2 Evaluation of Multi-Scalability 39

3.2.1 Experimental Results 39

3.2.2 Discussion 42

4 Vibration Control for Stable Grasping at High Speed 45

4.1 Introduction 45

4.2 Micromanipulation System 47

4.3 Vibration Analysis in the Microhand 50

4.3.1 Oscillation Observation 50

4.3.2 Frequency Analysis of Oscillation 51

4.4 Vibration Suppression of the End effectors 52

4.4.1 Structural Design to Increase Damping 52

4.4.2 Residual Vibration Control of the Right End Effector 54

5 Fast 3D Detection of Microobjects for High Speed Micromanipulation and Experimental Results 63

5.1 Materials and Methods 63

5.1.1 System Configuration 63

5.1.2 High Speed 3D Position Detection 64

5.2 Experimental Results and Discussion 73

5.2.1 High-Speed Manipulation 73

5.2.2 Discussion 76

6 Conclusions 78

Publications 92

List of Figures

1.1 Typical industrial robot (left) and high speed parallel mechanism industrial robot (right). 2
1.2 Gravitational force and the different adhesion forces as a function of the object radius. 3
1.3 In micro-scale, there are various size biological cells. 9
1.4 Concept of our goal: multilayered cell assembly (regeneration of tissues). 10
1.5 Duration for the pick-and-place of a microobject using various contact-micromanipulation techniques. 11

2.1 Single kinematics chain of parallel mechanism including prismatic, revolute, and spherical joints. 19
2.2 CAD model concept. 20
2.3 Parallel mechanism's geometrical model. 21
2.4 Workspace of current orientation in the X-Y plane. 23
2.5 Workspace of current orientation in the X-Z and Y-Z planes. 23
2.6 Different orientations on X-Z (left) and X-Y (right) planes. 25
2.7 Workspace results for different orientations (5° - blue, 45° - red, 90° - green) on the X-Z plane. 25
2.8 Workspace results for different orientations (0° - blue, 30° - red, 60° - green) on the X-Y plane. 27
2.9 System constraints (left) and intermediate part solution (right). 28
2.10 Intermediate part solution to obtain a more inclined resulting vector. . 28

3.1 System configuration. 32

3.2 Micromanipulator prototype. 32
3.3 Parallel mechanism control. 33
3.4 Accurate positioning flowchart. 36
3.5 Comparison of conventional (left) and proposed (right) coarse-to-fine motion strategies. 38
3.6 (a)-(b) Grasping task for 20 μm microspheres (c)-(d) transportation task for 60 μm distance (e)-(f) release process. 40
3.7 Manipulation of donor (left) and egg (right) cells. 42
3.8 Realization of the system's multi-scalability. 43

4.1 The microhand with the end effectors. 46
4.2 System configuration. 48
4.3 Position detection that is showing the contour, centroid and end effector tip. 51
4.4 Oscillation of both end effectors in x and y caused by 80 μm motion. . 52
4.5 Result of Fast Fourier Transform of x position of the left and right end effectors. 53
4.6 End effectors before (left) and after (right) structure modification. . . . 54
4.7 Vibration of right end effector after structure modification. 55
4.8 Vibration frequency of the right end effector is 60 Hz. 55
4.9 Block diagram of the vibration control system. 57
4.10 Vibration after compensation. 59

5.1 Detection of finger tip position. 64
5.2 Depth from border intensity variation algorithm. 66
5.3 Flow chart of high speed autopositioning. 68
5.4 Autopositioning process: a) Initial situation (target object and end effectors are out of focus), b) After autofocusing to target object, c) After autopositioning end effectors. 69
5.5 New minimum search. 70
5.6 Flowchart of Depth From Border Intensity Variation. 71

5.7 Flow chart of high speed manipulation. 74
5.8 High-speed grasping: a) Ready to start manipulation task, b) After moving the end effectors to target object, c) After grasping target object. 74
5.9 a) Ready for transportation, b) After transportation of target object, c) Releasing, d) End effectors moves away from target object. 75
5.10 1D microbeads string realization: a) Target positions, b) Before manipulation, c) After manipulation. 76

List of Tables

2.1 Motorized stages specifications 18
2.2 Comparison of theoretical and practical workspaces 24
2.3 Workspace results for different orientations of the end effector on the X-Z plane 26
2.4 Workspace results for different orientations of the end effector on the X-Y plane. 26
2.5 Workspace results before and after angle modification 29

3.1 Micromanipulator performance 44
3.2 Comparison to similar manipulation systems 44

4.1 Vibration and settling time after vibration suppression 60

1

Introduction

1.1 General Background

“What I want to talk about is the problem of manipulating and controlling things on a small scale” said Richard Feynman in his great talk “There is Plenty of Room at the Bottom” given on December 1959 at the annual meeting of the American Physical Society. Today, after five decades, micromanipulation still stays as a challenging issue.

Three aspects of micromanipulation are manipulator, target object, and motion resolution. The manipulator and target object could be in micro or macroscales, however, at least, motion resolution should be in the micrometer range to define the scale of the control as micromanipulation.

Various micromanipulation systems have recently been designed and used for applications such as assembling micromachines, assisting in microsurgical operations, and manipulating biological cells. Accurate and precise bio-micromanipulation is still a task of utmost importance in biomechanics, microbiology, and genetics. [1].

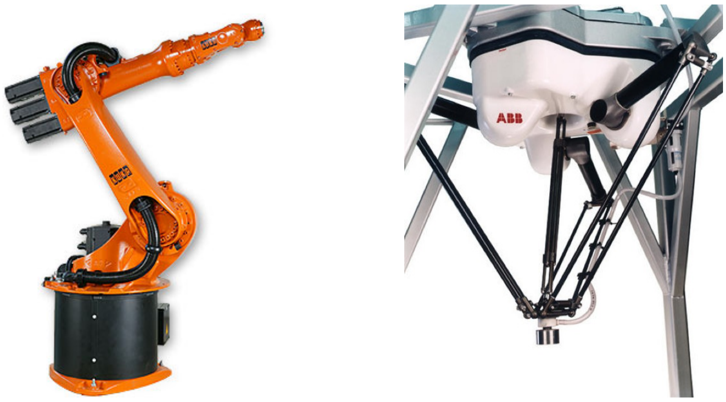

Figure 1.1: Typical industrial robot (left) and high speed parallel mechanism industrial robot (right).

1.1.1 Manipulation in Macro and Micro Scales

One of the best example of the manipulation systems in macroscale is industrial robots which are mostly serial mechanisms (Fig. 1.1). According to International Federation of Robotics' 2012 report, industrial robots started to be part of factories in early 1960s [2]. These robots started to be comman in Japan in 1970s and help to manufacturing of goods in a reliable way. It is accepted that, one of the effective parameters for Japan to develop the economy in short time is utilization of these industrial robots. Currently, there are more than 1.1 million industrial robots in the factories all over the world as a key component of automation for manufacturing. There are several reasons why industrial robots are very significant as a manipulator in automation:

1. Improving quality of the work
2. Increasing product output rate
3. Increasing product quality and consistency
4. Increasing flexibility in product manufacturing
5. Reducing operation cost

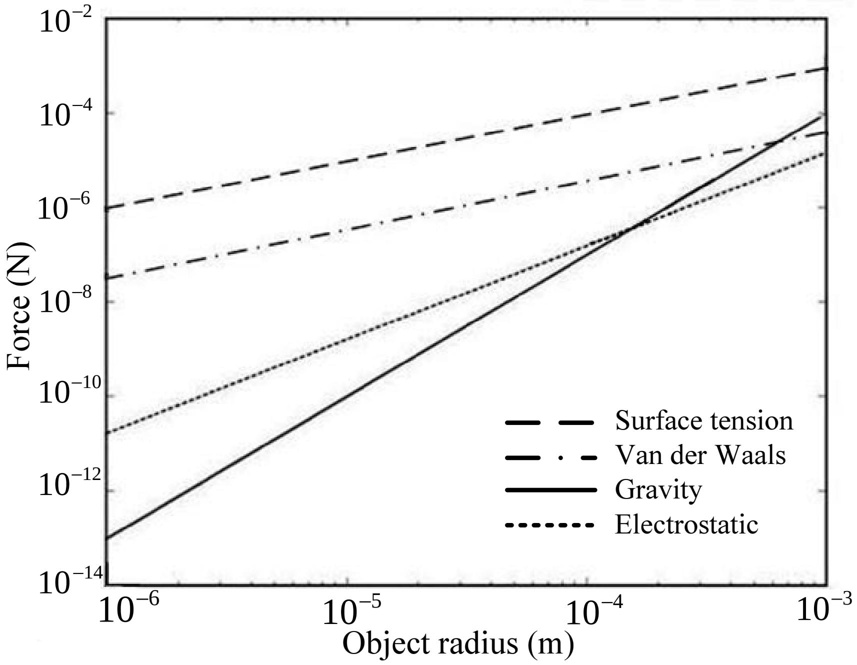

Figure 1.2: Gravitational force and the different adhesion forces as a function of the object radius.

First high speed picking industrial robot (ABB FlexPicker) developed in 1998 which can pick 120 objects in a minute using image technology. The interesting feature of this robot was being parallel mechanism instead of serial links, as parallel structure is more suitable for precise and repeatable motions at high speed as seen in Fig. 1.1.

On the other hand, various manipulators for microscale handling have been proposed; and particularly in 1980s and 1990s, a lot of studies were carried out about micromanipulation sytems and techniques. In the last decade, micromanipulation became more appealing to researchers due to be a potantial solution for various microbilogy issues. However before moving on to micromanipulation systems, it is necessary to understand pysics in the microscale.

Dynamics of microscopic objects are different from macroscale objects. As length(l) of objects decrease from macro to microscale, surface forces (l^2) begin to dominate body forces (l^3). Because gravitational forces are proportional to the object volume whereas adhesion forces are proportional to object surface, thus, adhesion become dominant compare to gravitational force in the microscale as seen in Fig. 1.2 [3]. The adhesion forces include van der Waals forces, electrostatic forces, and surface tension forces [4].

Due to stronger adhesion forces in micro world, releasing of the object is more difficult than grasping them. This micro world physics offer new challenges for micromanipulation. Therefore, several micromanipulation methods have been developed in the last two decades.

1.1.2 Micromanipulation Methods

Needs in the biotechnology field and challenges in the microscale result in various methods to manipulate microobjects. Micromanipulation systems can be classified mainly non-contact and contact manipulation which will be explained in the following sections. Details of each method can be found in [5].

1.1.2.1 Non-Contact Micromanipulation

In non-contact micromanipulation, force is applied to the target microobjects without any mechanical contact [6].

The optical tweezers are one of the non-contact micromanipulation systems that use a highly focused laser beam to provide the force, which is commonly piconewton level, to hold and move the microscopic objects. However long holding time might damage the target biological object due to heat [7–9].

Dielectrophoresis (DEP) is another non-contact manipulation which a force is exerted on a dielectric particle using non-uniform electric field. The effect of the the force depends on the medium and microobjects' properties. Therefore, DEP can manipulate microobjects with selectivity [10–12].

Fluid flow manipulation is referred as non-contact manipulation which is for single-cell applications. It is a suitable method for biomedical field due to non-invasive behaviour. Transportation and other manipulation tasks of various size cells can be achieved with this technique [13]. The drawbacks of this technique are requirement of high accuracy micropumps and the difference between speed of particles and liquid.

Non-contact micromanipulation methods have also been proposed to handle microbiological objects by utilizing other kinds of forces such as acoustic [14–17] and aerodynamic forces [18, 19].

1.1.2.2 Contact Micromanipulation

Contact-micromanipulation involves the use of an end effector to manipulate microobjects mechanically. In the case of biological objects, operators manage to manipulate them by the micromanipulators with the two-dimensional image from the microscope, as depth information is not available with the optic microscope. Thus, contact micromanipulation is suitable when the object is large enough. i.e., more than a few micrometers [20].

On-Chip Micromanipulation Systems

Recently, integration of the microtools into a single chip is feasible. Magnetic driven microtools (MMT) were developed to provide many microfluidic functions, such as those of manipulation, sorting, dispensing, etc. [21, 22]. They can also be used for more complicated tasks such as removal of zona pellucida [23] and enucleation of oocyte [24]. The microfluidic chip itself can also be used as a microtool in cell-cutting

[25]. Multiple functions can be integrated into a single chip to perform sophisticated bio-applications such as automated mammalian cell cloning [26].

Off-Chip Micromanipulation Systems

Conventional contact micromanipulation systems are very advantageous, as these systems can utilize sophisticated microtools.

Atomic force microscopy (AFM) is a technique for analyzing the surface of a rigid material at the nanoscale. In addition to its 3D sensing capability, two cantilever tips can also be used to manipulate microobjects in three-dimensional space [27].

Since adhesion force often causes the sticking of the microobject to the end-effector, a sophisticated microgripper with a pushing mechanism between the gripping arms was also introduced to release microobjects successfully [28].

Micropipettes is a an example of contact manipulation and very useful for manipulationg biological objects. They can be used to aspirate or hold cells to deposit them at desired position for single cell manipulation and cell assembly tasks [29] or to immobilize a moving sperm, then aspirate it, and finally inject it into an oocyte [30].

A thermal responsive gel probe was also prepared to manipulate microobjects. The thermoresponsive polymer solution around the probe tip can be gelled by turning on the microheater at the tip; and cells near the probe tip can be handled by the produced thermal gel; and turning off the heater for releasing task takes place [31].

A two-fingered microhand is a very useful contact micromanipulator. The two microfingers are fabricated simply by pulling glass rods and can be used to handle microobjects in three-dimensional space. The use of the two microfingers is similar to using chopsticks; thus, it facilitates dexterous motions such as rotation, cell's nucleus extraction [1]. In addition, it can be useful for manipulating multi-sized microobjects [32, 33].

In this study, target applications are manipulation of biological cells and creation of 3D structure from single-cell. For this purpose, two-fingered microhand is the best candidate among above-explained techniques as dexterous handling in 3D is required for cell manipulation and assembly tasks.

1.2 Statement of the Problem

In micromanipulation field, we concentrate on two main issues. First, to manipulate different size microobjects precisely in a large workspace, how to design a micromanipulation system. The purpose here is the proposing a new concept which is multi-scalable microhand system. Second, to utilize the microhand in complex bio-applications, e.g., 3D cell assembly, how to speed up the system and how to achieve stable control at high speed.

1.2.1 Multi-Scalability

The realization of a multi-scalable micromanipulator that can handle multisized microobjects and transport them with precise positioning in a large workspace is crucial. When performing a cell fusion task, the micromanipulator should be able to carry a bovine egg cell, which is about 100 μm, and a bovine donor cell with a size of 10 μm and have them contact each other [26]. To fulfill this task, the system should have the ability to carry biological cells of different sizes for long distances (a few hundred μm) and position them precisely (sub-micron) to have them come in contact. The same features are necessary for the assembly of MEMS and MOEMS devices [34–36].

To achieve a multi-scalable microhand system that is compatible with various microapplications, i.e., a general-purpose microhand, the following two features are required: First, the microhand end effector should have a large workspace with a high resolution for grasping different-sized microobjects. Second, a large workspace with a precise positioning function is necessary for the transportation of microobjects.

For the first feature, previous studies have shown that most micromanipulators have been designed as task-specific systems to manipulate particular microobjects [37–40]. Due to workspace limitations or low resolution, these systems can be used only for the manipulation of a particular size of object, which limits their applications. There are, in fact, only a few studies of microhands that manipulate multisized microobjects. The manipulation of borosilicate glass spheres, which are several sizes from a few microns to 17 μm [28], and polystyrene spheres, which are various sizes from 20 μm to 100 μm [41], has been achieved. In order to realize a general-purpose micromanipulator that is compatible with various microapplications, however, it is critical to achieve manipulation of various-sized microobjects from a few microns to over a hundred microns. In micro environment, all kind of objects have different size as seen in Fig. 1.3. Bacterias are just 1-2 μm, sperm, yeast cell, fibroblast, lymphocytes are about 10 to 15 μm whereas egg cells, megakaryocytes and some kind of nerve cells are about 100 μm or bigger than that. Thus, multi-sized objects manipulation ability is important.

For the second necessary feature, which is the transportation of microobjects up to a millimeter-scale with sub-micron precision, creating a large workspace with high resolution is important. One of the strategies available to do so is the combination of coarse motion and fine motion functions in the same microsystem [42, 43]. In dual stage systems, the coarse actuator provides a large workspace while the fine actuator makes precise motion possible, so the disadvantages of one actuator can be compensated for by the advantages of the other actuator. The time lag is, however, a disadvantage of this strategy. The coarse stage moves the end effector to the target position and stops, then the fine stage compensates for position error, so there is a delay between

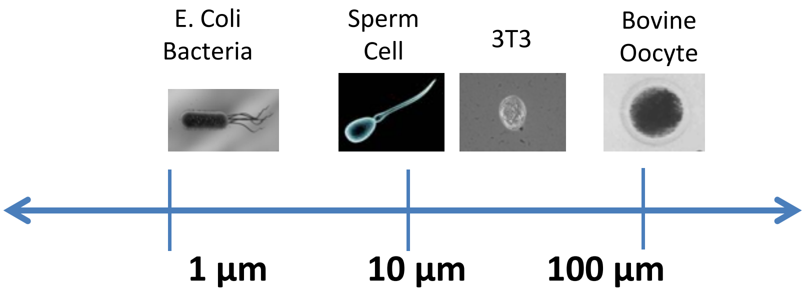

Figure 1.3: In micro-scale, there are various size biological cells.

coarse and fine motions [42]. In addition, most of the time, the system should move the end effector very slowly to achieve accurate positioning through many template matching cycles [43].

In brief, two challenges to achieve multi-scalability in a micromanipulation system are as follows:

- How to design a microhand to manipulate different size microobjects;
- How to realize large transportation ability with high precision.

Multi-scale manipulation ability would be particularly useful in terms of performing wide range of different tasks. And this ability increases flexibilty in micromanipulation and assembly.

1.2.2 Micromanipulation at High Speed

Regenerative medicine is the process of regenerating human cells, tissues or organs to replace damaged ones [44]. Several bio-engineering approaches such as cell sheet engineering [45] and bio-printing [46, 47] have been proposed to regenerate cell tissues. Aside from these techniques, the pick-and-place method for cell-assembly has drawn

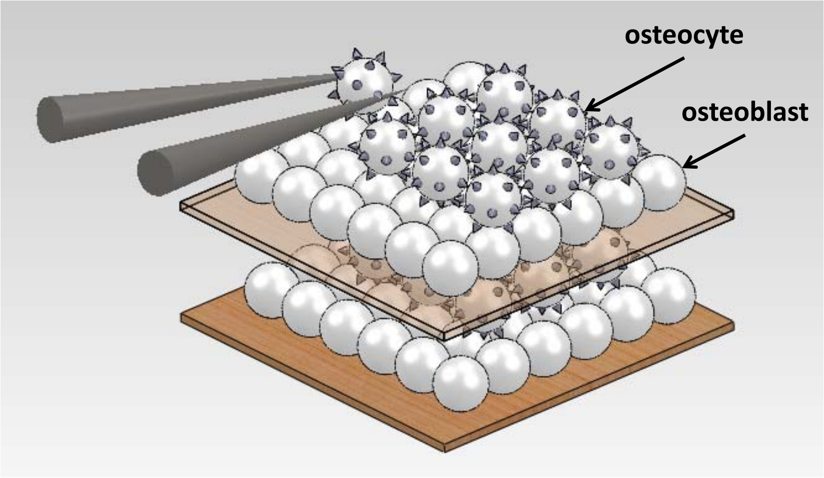

Figure 1.4: Concept of our goal: multilayered cell assembly (regeneration of tissues).

much attention [29, 31].

For this method, a micromanipulation system is an indispensable tool. When regenerating cell tissues, our ultimate goal is to achieve multi-layered cell assembly by using a two-fingered micromanipulation system as illustrated in Fig. 1.4. The first step towards this goal is the automated pick-and-place operation of the cells.

High speed is a necessary requirement for such a micromanipulation system, because of the presence of a vast number of cells and their restricted life span. The last two decades have witnessed significant efforts in the realization of micro-scale automated robotic operation [48–56]. Autonomous micromanipulators were designed with attention to the range of motion and the accuracy, and less attention to the speed of the motion.

Recently, Xie et al. achieved the automated pick-and-place operation of microspheres in 48 seconds; 20 seconds of this duration were used for the grasping of the target object [27]. Lu et al. succeed the pick-and-place of biological cells in 15 seconds [29]. Nguyen et al. realized the first step of pick-and-place task, which is grasping, of

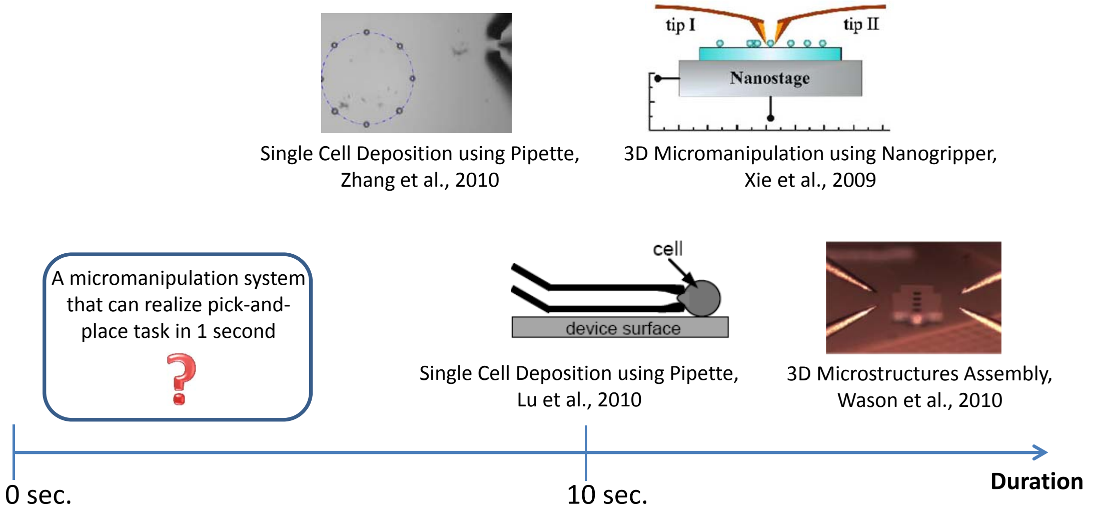
Single Cell Deposition using Pipette,
Zhang et al., 2010
tip I
tip II
Nanostage
3D Micromanipulation using Nanogripper,
Xie et al., 2009
A micromanipulation system that can realize pick-and-place task in 1 second
?
cell
device surface
Single Cell Deposition using Pipette,
Lu et al., 2010
3D Microstructures Assembly,
Wason et al., 2010
0 sec.
10 sec.
Duration

Figure 1.5: Duration for the pick-and-place of a microobject using various contact-micromanipulation techniques.

various size microbeads(20, 55, 96 μm) in 1.5 seconds [32]. Zhang et al. achieved the automated pick-and-place operation of microspheres with a speed of 6 seconds/sphere which has been the highest speed reported in the literature [57]. These studies made a gradual progress in the field of high-speed micromanipulation. However, a micromanipulation system utilizing the pick-and-place method at adequately high speed for tissue engineering has yet to be constructed (Fig. 1.5).

To achieve high-speed micromanipulation, not only fast actuation but also high-speed and stable control of the micromanipulation system is required. The following difficulties should thus be overcome. First, to start the pick-and-place task, knowledge of the 3D positions of both the end effector and the target microobject should be obtained fast and accurately. However, under standard light microscopy, vision is two-dimensional and depth information is not feasible. Second, researchers mostly focus on precise control more than high speed, as rapid motions may cause significant unwanted disturbances to the microenvironment. When the actuators of the microhand move at normal speed, the vibration of the end effector is in the imperceptible level;

however, when the actuators move faster, the system faces bigger acceleration and deceleration, thus the force applied to the system increases. As the vibration of the end effector is proportional to the applied force, during the high-speed grasping task, the residual vibration of the end effector increases and makes the manipulation process longer and less successful.

The difficulties connected with achieving high-speed and stable control of a micromanipulation system can be summarized as follows:

- Achieve fast and accurate measurement of 3D positions of both the target microobject and the end effector;
- Control the vibration of the end effector caused by high speed motion.

The micromanipulator chosen in this study is a two-fingered microhand [1, 33] since it is a potential tool for micromanipulation. Since they are fabricated by pulling glass rods, the two microfingers of the microhand are transparent and biocompatible. By using this microhand dexterous micromanipulation such as cell rotation [1], and measurement of mechanical properties of a living cell [58, 59] can be performed.

1.3 Main Contributions

1.3.1 Concept of Multi-Scalability

Most actuators that are used for microhands have high resolution and a small workspace, e.g., PZT actuators. In some cases, expansion mechanisms can be integrated in the system to increase workspace but decreases resolution as a trade-off [60]. Entire micromanipulation system should be compact enough to be put on the stage of the existing microscope. The microhand itself should therefore be designed very carefully to achieve a large workspace. In our previous study, we designed a parallel mechanism for grasping and releasing microobjects. It was optimized to realize the best configuration for the largest workspace under ideal conditions, and the experimental workspace result was 640 x 590 μm [61]. When this parallel mechanism was integrated in an actual micromanipulation system, however, usable workspace became 45 x 22 μm [62]. Workspace optimization should therefore be conducted considering the actual setup and searching for the appropriate orientation of the end effector. For this, the workspace analysis of the parallel link mechanism should be done, since the relationship between design parameters and the workspace, and behaviour of the microhand throughout the workspace, is not intuitive by any means [63]. In this study, the workspace of the parallel mechanism has been optimized with the help of inverse kinematics by modifying the orientation of the end effector, which is fixed to the end of the parallel mechanism, to meet the condition of handling target objects of various sizes in microscale.

For the second necessary feature, which is the transportation of microobjects up to a millimeter-scale with sub-micron precision, creating a large workspace with high resolution is important. One of the strategies available to do so is the combination of coarse motion and fine motion functions in the same microsystem. In this study, the conventional coarse-to-fine motion strategy has been improved to achieve fast precise positioning throughout a large workspace and to remove the time lag between coarse and fine motions.

1.3.2 Successful Control of Microhand at High Speed

To tackle above-mentioned difficulties of high-speed micromanipulation and to perform the pick-and-place task in 1 second, we propose a new fast detection algorithm, which will enable us to obtain the 3D positions of the end effectors and the target microobject. In this research, a top-down scanning of the target microobject and microfingers is performed by using a piezo actuator that can move the objective lens over a distance of up to 100 μm along the optical axis at 15 Hz. The actuator moves the objective lens with a 1 μm step, while the high-speed camera captures the image at 2,000 frames per second. A stack of 90 images captured at consecutive and equally spaced focal planes is thus obtained. By searching for the index of the image in which the target object or the microfinger is best focused, its z-position is obtained.

In addition, to realize successful grasping of microobjects at high speed, it is necessary to analyze the vibration behavior and develop an efficient suppression method. Tao et al. modeled the residual vibration and used an acceleration smoother to suppress the vibration of the SCARA robot arm [64]. In the microrobotics field, most of the studies focus on the vibration suppression of piezo actuators, as the oscillation is the natural result of applying voltage to the piezo material [65–68]. However, the residual vibration suppression in a microhand has not been studied yet.

To achieve successful manipulation at high speed, we decrease the vibration amplitude and duration in two steps: first we increase the stiffness of the microhand by increasing the tickness of the end effectors; then, to further decrease the residual vibration, we apply an appropriate control method. As we can predict the behavior of the vibration (frequency, amplitude, settling time, etc.) for a specific acceleration, we implement the feedforward control to suppress the vibration in the system.

We focus on the above-mentioned difficulties of high-speed micromanipulation. To grasp the object, an accurate and fast 3D detection algorithm is proposed. To achieve fast and stable manipulation, the residual vibration in the microhand is reduced.

1.4 Organization of the Thesis

This chapter presents a brief introduction of micromanipulation that will be discussed in details in the following chapters. First, the general background of the physics in the microscale and micromanipulation is introduced, followed by a description of the main problem of the thesis. Then, the main contributions achieved for multi-scalability and high-speed micromanipulation are presented. Finally, this section provides the outline of the thesis. The content of the rest of thesis is organized as follows:

Chapter 2 introduces the workspace optimization of the microhand for multi-sized microobjects manipulation. In order to utilize the system for different size objects handling in the micro-scale, workspace of the parallel mechanism is analyzed by inverse kinematics. In order to achieve the biggest flat workspace, workspace optimization is conducted via analyzing the workspace for different orientations of the end effector. At the end of optimization procedure, the best orientation for the largest workspace has been realized.

Chapter 3 describes, on the stage of the inverted microscope, which is very limited area, how to achieve a large workspace for the transportation of microobjects and keep precision high simultaneously. For this, coarse to fine manipulation strategy proposed. By implementing coarse motion stage and fine motion stage into the micromanipulation system and by using vision as a feedback tool, we achieved large workspace with precise motion ability. Moreover, to improve conventional coarse to fine motion strategy, time lag between coarse and fine motion is removed by using visual feedback. At the end of the chapter, three different experiments are added to demonstrate multi-scalability concept.

Chapter 4 introduces how to control the residual vibration at high speed manipulation task. When the end effectors of the micromanipulation system move at high speed, vibration data is gathered and analyzed. Then to suppress the residual vibration, the stiffness of the structure is increased and then, as we can predict the behavior of the vibration (frequency, amplitude, settling time, etc.) for a specific acceleration, we implemented the feedforward control.

Chapter 5 describes how to obtain depth information for the end effector and the target object at high speed. A top-down scanning of the target microobject and microfingers is performed by using a piezo actuator that can move the objective lens. And the information of the exact place of the center of the object and end effector is obtained. And single microobject manipulation at high speed is shown as an experimental result. Furthermore, 1D array (string) of three microbeads is carried out to show high speed control ability of the system.

The last chapter, Chapter 6, concludes the thesis with a brief summary of achievements, discussion of the remaining issues and possible directions for future research.

2

Workspace Optimization for Manipulation of Multi-sized Microobjects

2.1 System Concept

At the beginning of the design process, the system concept has been defined as a micromanipulator that achieves large workspace and precise motion at the same time. This system is composed of two main parts: lower and upper modules.

The lower module is for global motion, that is, the movement of both end effectors that achieves the transportation of target objects and the positioning of the microhand. Two motorized stages –coarse (Sigma-Koki, TSD-805S) and fine (Sigma-Koki, SFS-H60XYZ) stages– form the lower module and help realize the large workspace and precise motion necessary for the transportation task. Specifications of fine and coarse stages are listed in Table 2.1. We use these two stages to move both end effectors for long and coarse motions, i.e., for traveling long distances (micro and millimeter-scales), and for short and fine motion (nano and micro-scales). This enables us to

Table 2.1: Motorized stages specifications

	Fine Stage	Coarse Stage
Travel(mm)	0.1(X,Y,Z)	25(X,Y),10(Z)
Resolution(μm)	0.01	1
Accuracy (μm)	0.1	17
Repeatability (μm)	0.15	2
Max. Speed (mm/s)	2.3	0.1

achieve precise positioning when grasping and releasing tasks are executed.

The upper module is for local motion, i.e., the movement of the upper end effector. Local motion achieves the grasping and release of different-sized target objects. One manual stage for adjusting the upper end effector with respect to the lower one and one parallel link mechanism for manipulating different-sized objects form the upper module and realize a large workspace for the grasping task. The manual stage moves 6 mm in the X, Y, and Z directions with a resolution of 3 μm. The parallel link mechanism includes 3 piezoactuators as prismatic joints that can be extended up to 40 μm. Workspace optimization is realized by changing end effector's orientation so that it has the largest feasible workspace for a fixed-size end effector, as explained in section 2.2. In addition to its simple compact configuration, the parallel mechanism has the advantages of high speed, high accuracy, and high rigidity. It has simple joint mechanisms using a flexure hinge as a revolute joint and a wire as a spherical joint in each link, as shown in Fig. 2.1. The mechanism has a 3-DOF end effector (two rotational and one translational motion), and has no singular point in its actual workspace. Three linear piezoelectric actuators (NEC TOKIN, AE0203D16) are arranged on a base plate so that their displacement is vertical to this plate. This arrangement has two advantages: first, the movable parts of the finger can be rather light, and, second, workspace along

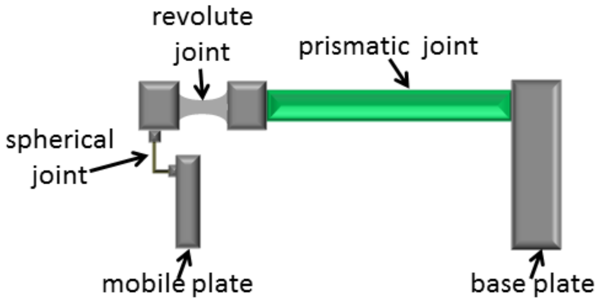

Figure 2.1: Single kinematics chain of parallel mechanism including prismatic, revolute, and spherical joints.

the Z axis with reference to the base coordinate frame is its largest.

After the design concept is decided, a CAD model of the micromanipulator is prepared, as shown in Fig. 2.2.

2.2 Workspace Analysis

For the manipulation of different-sized microobjects, parallel mechanism workspace should be at least 100 μm for the X direction, which is the direction of the motion of the end effector when grasping and releasing tasks are carried out. The manipulation of large microobjects such as 97 μm diameter bovine cells will be thus achievable. In addition, accuracy should be at a sub-micron level for the manipulation of objects having a size of only a few microns, e.g., fibroblasts and bacteria.

The upper end effector is fixed to 3-DOF (prismatic-revolute-spherical (PRS) joints) parallel mechanism that was analyzed to understand upper end effector workspace. Details of workspace analysis and the workspace optimization process are as follows.

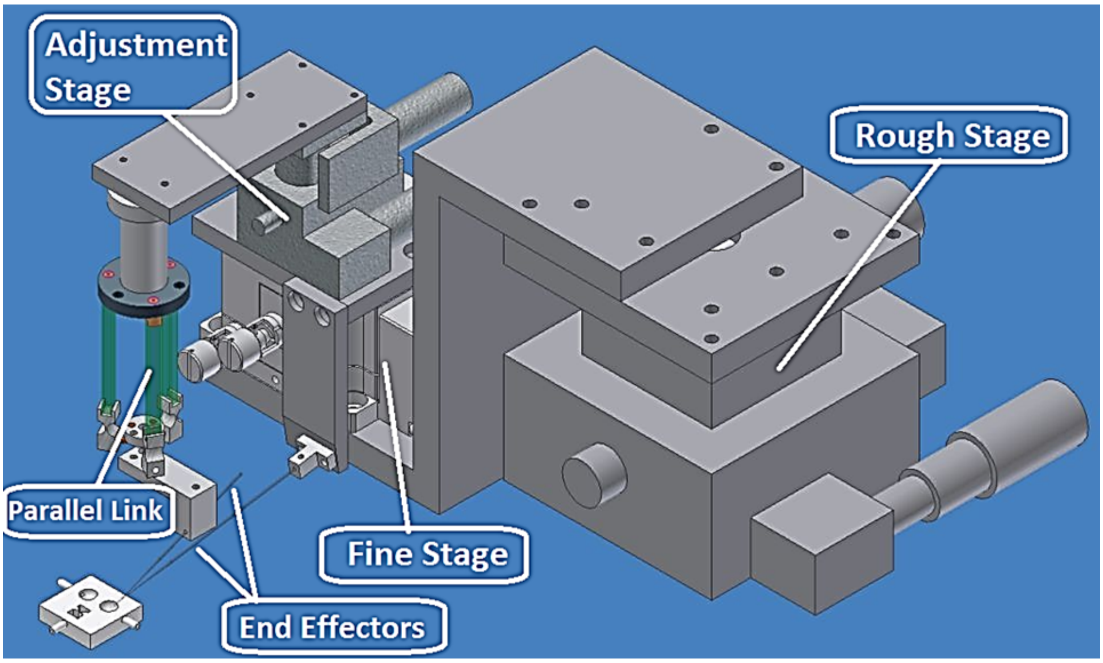

Figure 2.2: CAD model concept.

Although forward kinematics is more suitable and easier way to calculate workspace of serial mechanisms, unfortunately forward kinematics' equations are highly nonlinear and cannot be decoupled to get a closed form solution for parallel mechanisms. Therefore, inverse kinematics is used to calculate workspace. By using inverse kinematics, we attempted to realize workspace by checking feasible extensions of parallel mechanism's parts, which is up to 40 μm. Single kinematics chain of parallel mechanism, which includes Prismatic, Revolute and Spherical joints, and mechanism's geometrical model can be seen in Fig. 2.1 and 2.3. The procedure of calculation is as follows: Tip position of end effector (Pe) will be given. By the help of this information and by using Newton-Raphson method (2.1) we can calculate position of mobile plate center (Pc).

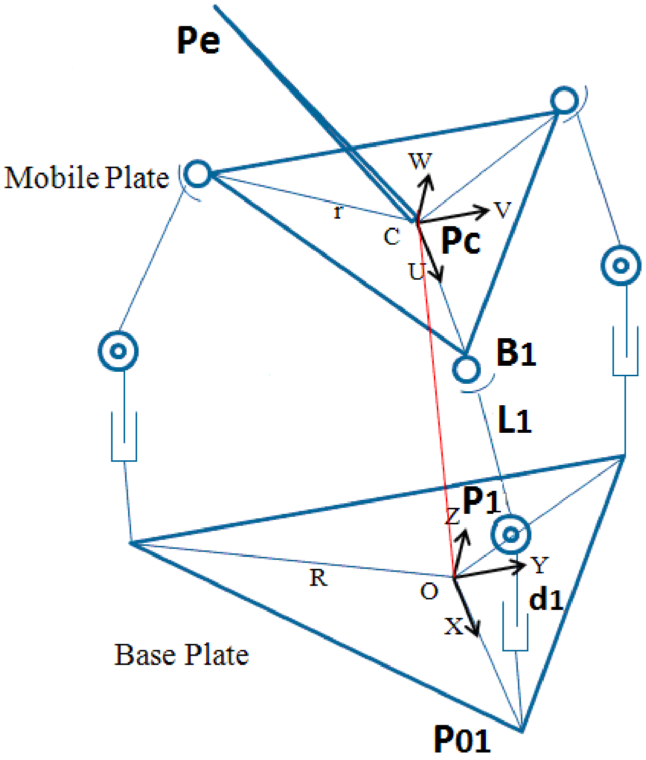
Pe
Mobile Plate
W
V
r
C
Pc
U
B1
L1
P1
Z
Y
R
O
d1
X
Base Plate
P01

Figure 2.3: Parallel mechanism's geometrical model.

$$\begin{bmatrix} Pcx \\ Pcy \\ Pcz \end{bmatrix}^{k+1} = \begin{bmatrix} Pcx \\ Pcy \\ Pcz \end{bmatrix}^{k} - J^{-1}(Pcx, Pcy, Pcz)^{k} \times f(Pcx, Pcy, Pcz)^{k} \tag{2.1}$$

After a few iterations, mobile plate center can be found. Then, the transformation matrix, which includes mobile plate center position (Pc) and rotation matrix (ROT) (2.2), should be used to calculate mobile plate frame referred to fixed base frame.

$$Pc = \begin{bmatrix} Pcx \\ Pcy \\ Pcz \end{bmatrix} \quad ROT = \begin{bmatrix} Ux & Vx & Wx \\ Uy & Vy & Wy \\ Uz & Vz & Wz \end{bmatrix} \tag{2.2}$$

By the help of (2.1), (2.2) and constrains of revolute joints, extension of three piezo actuators can be found.

By the inverse kinematics method, workspace of current orientation, which means current position of end effector that is 27.5° in the X-Z plane, has been realized through searching 1000 x 1000 x 1000 μm volume for possible workspace. As a result, workspace of current orientation can be seen in Fig. 2.4 for the X-Y plane,and in Fig. 2.5 for X-Z and Y-Z planes.

In Fig. 2.4,and 2.5, it can be seen that workspace is 330 μm in the X direction, 310 μm in the Y direction and 620 μm in the Z direction. Comparison of theoretical and experimental workspaces can be seen in Table 2.2. The practical X range is about 15 percent less than that of theoretical value and practical Y range is 17 percent less than that of theoretical value. The small difference between theoretical and experimental workspaces is due to the use of pin flexure joint as a revolute joint and wire as a spherical ball joint.

At the end of current orientation's workspace analysis, we came up with two questions. Firstly, as it can be seen in Fig. 2.5, entire workspace is inclined so when we

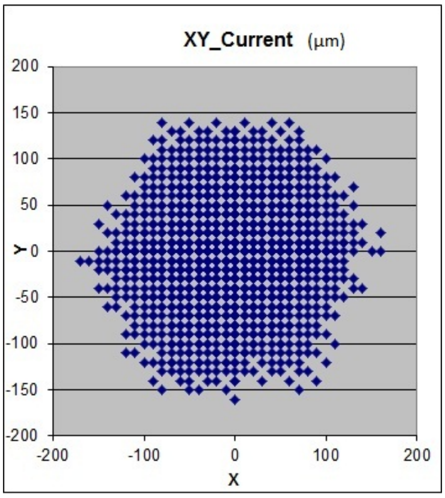

Figure 2.4: Workspace of current orientation in the X-Y plane.

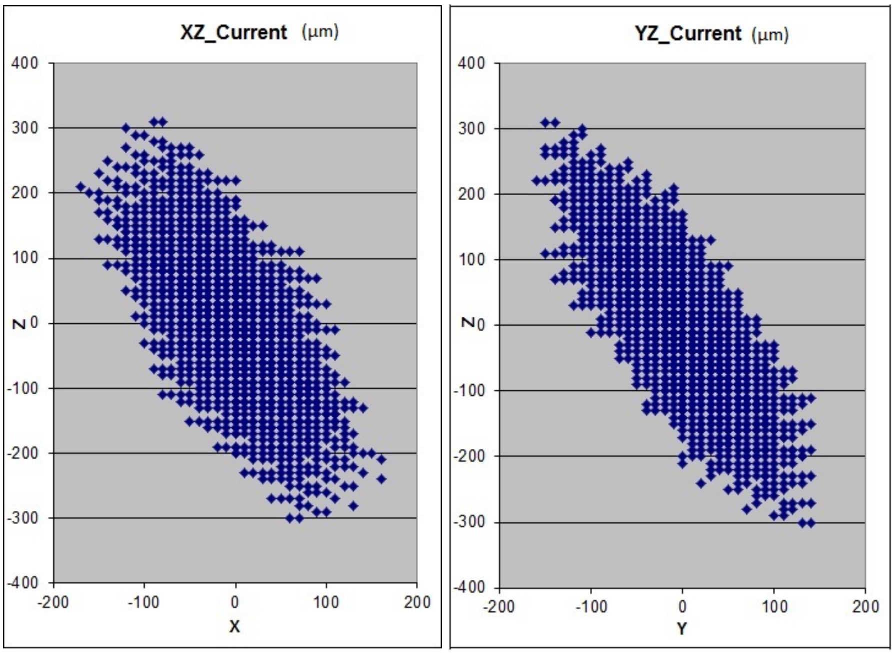

Figure 2.5: Workspace of current orientation in the X-Z and Y-Z planes.

Table 2.2: Comparison of theoretical and practical workspaces

Workspace	x [um]	y [um]
Theoretical	330	310
Experimental	280	255

move our end effector in the X and Y directions while Z is constant, we can use less than half of the workspace. For current orientation, while Z is constant, experimental workspace is 45 μm for X and 22 μm for Y directions. To be able to grasp different size microobjects, X direction's workspace is the most important parameter and 45 μm is not big enough. As it mentioned before, for the target application, workspace of X direction should be at least 100 μm. So, the question is can we use workspace more efficiently, in other words, can we make it less inclined? Secondly, can we increase this workspace? To find answers of these problems, workspace optimization is carried out.

2.3 Workspace Optimization

The purpose of workspace optimization is to decide the orientation of the end effector for the largest horizontal workspace. Because inclined workspace cannot be used efficiently, we sought a flat workspace; whose X axis can be used as a reference. To find the largest flat workspace, results were obtained about workspace of different orientations by checking two different planes, as shown in Fig. 2.6.

On the X-Z plane, which is a side view of the parallel system, different orientations were checked, as shown in Fig. 2.6 (left). Workspace results for different orientations are listed in Table 2.3 and shown in Fig. 2.7.

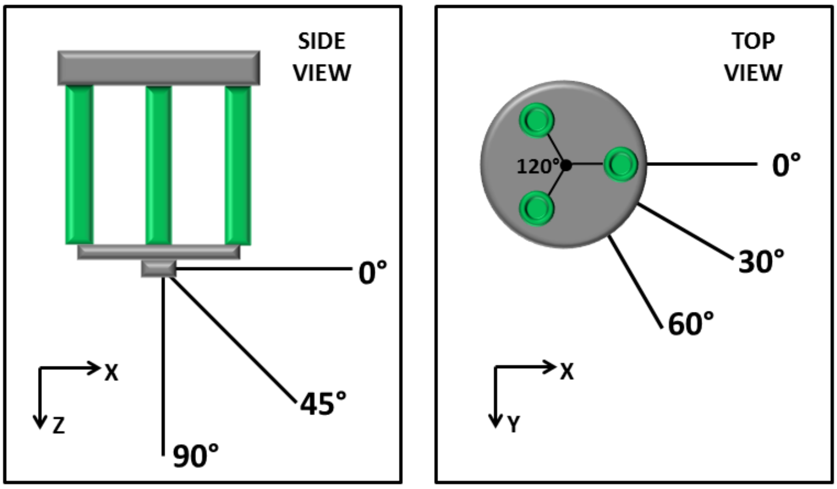
SIDE VIEW
0°
45°
90°
X
Z
TOP VIEW
120°
0°
30°
60°
X
Y

Figure 2.6: Different orientations on X-Z (left) and X-Y (right) planes.

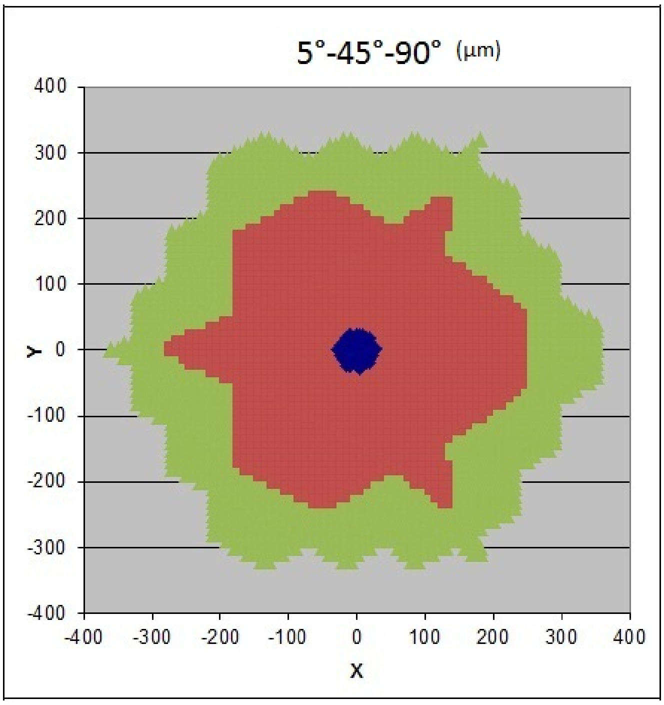

Figure 2.7: Workspace results for different orientations (5° - blue, 45° - red, 90° - green) on the X-Z plane.

Table 2.3: Workspace results for different orientations of the end effector on the X-Z plane

X-Z plane	X (μm)	Y (μm)
0°	0.6	0.8
45°	530	480
90°	720	640

Table 2.4: Workspace results for different orientations of the end effector on the X-Y plane.

X-Y plane	X (μm)	Y (μm)
0°	530	480
30°	510	480
60°	540	480

On the X-Y plane, which is the top view of the parallel system, different orientations were checked, as shown in Fig. 2.6 (right). Workspace results for different orientations are shown in Table 2.4 and Fig. 2.8.

Workspace analysis results for different orientations are summarized as follows: if we change the orientation downward on the X-Z plane, workspace increases. The largest workspace is realized at 90°. If we change the orientation on the X-Y plane, the workspace size hardly changes. In addition, during the workspace analysis process, we found that the inclination of the workspace X axis is inversely proportional

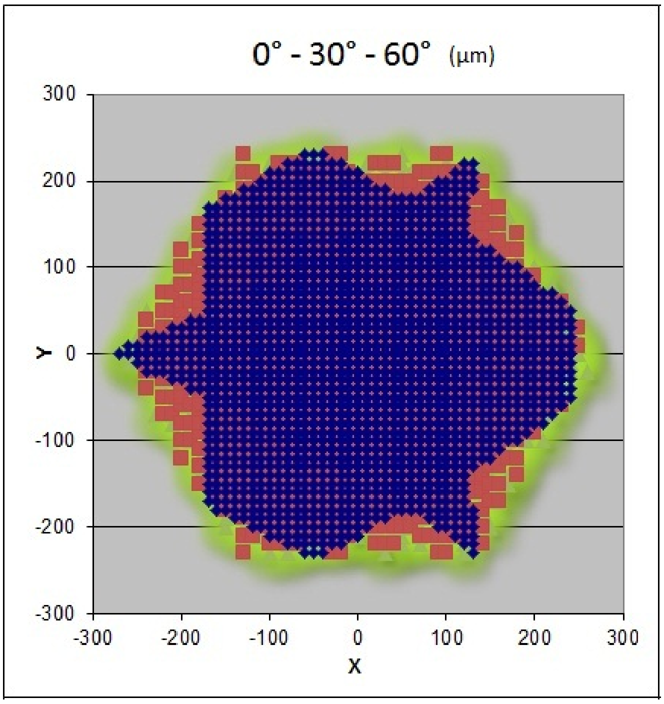

Figure 2.8: Workspace results for different orientations (0° - blue, 30° - red, 60° - green) on the X-Y plane.

to the orientation angle of the end effector on the X-Z plane. For 0° orientation, the slope of the X axis is 89.8° and for 90° orientation, it is 0.7°, which is close to a flat plane. Hence, to have a large flat workspace, the end effector should form a 90° angle on the X-Z plane. If this is not feasible because of micromanipulation constraints, the orientation of the end effector on the X-Z plane should be as close as possible to 90°.

Although a 90° orientation, normal to the ground, is the best angle for obtaining the largest flat workspace, there are two main constraints that should be considered. First, to observe the micromanipulation process with an inverted microscope, the end effector should be placed between the light source and the lens, for which 90° orientation is not possible, as shown in Fig. 2.9 (left). Second, in order to avoid breaking the glass finger during 3D motion of the system, the end effector should not be normal to the ground. When considering these two constraints with respect to workspace op-

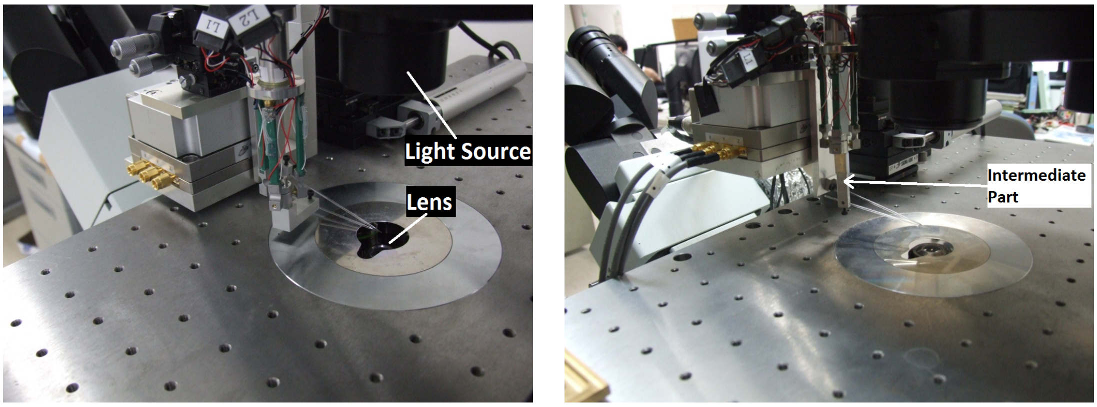
Light Source
Lens
Intermediate Part

Figure 2.9: System constraints (left) and intermediate part solution (right).

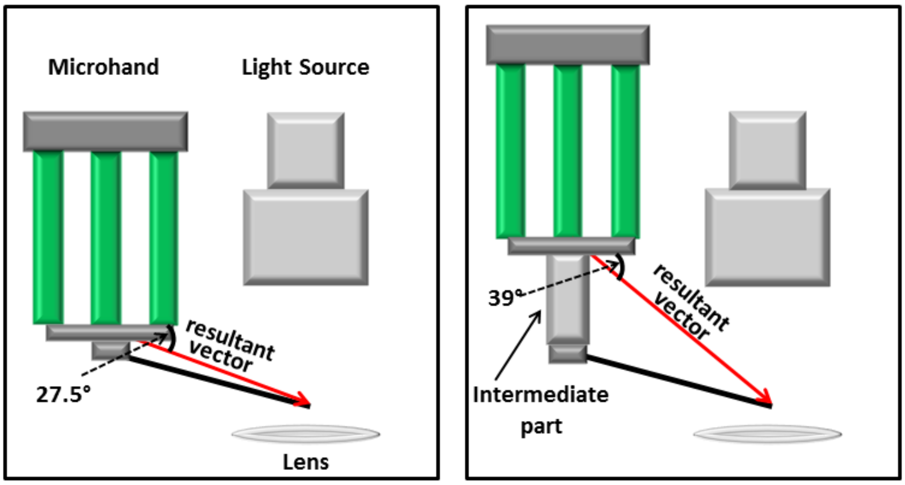
Microhand
Light Source
resultant vector
27.5°
Lens
39°
resultant vector
Intermediate part

Figure 2.10: Intermediate part solution to obtain a more inclined resulting vector.

Table 2.5: Workspace results before and after angle modification

	x [um]	y [um]
former (27.5°)	45	22
latter (39°)	132	40

timization results, we propose using an intermediate part as a solution, as illustrated in Fig. 2.9 (right) and in Fig. 2.10, placed between the parallel link and the end effector to obtain a more inclined resultant vector. A longer intermediate part means closer orientation to 90° for the resulting vector. Hardware limitations, system setup, and a vibration problem have to be considered, however, when deciding the maximum feasible length of the intermediate part. After these limitations were considered, the length of the intermediate part was set to 3.5 cm. With the optimized intermediate part, we were able to realize a 39° angle on the X-Z plane as the feasible degree closest to 90° orientation, as shown in Fig. 2.10.

After we consider workspace inclination for 39° orientation, if we keep the depth, which is the Z direction, fixed, then we can move our end effector 132 μm in the X direction and 40 μm in the Y direction with an observable resolution of 0.1 μm. Hence, with this workspace size, the ability of the microhand to manipulate different-sized microobjects was improved from 1-45 μm to 1-132 μm.

3

Coarse to Fine Manipulation Strategy and Experimental Results

3.1 System Construction

3.1.1 System Configuration

Fig. 3.1 shows the configuration of the micromanipulation system, in which, the main part is a two-fingered micromanipulator. Details of the actual system are shown in Fig. 3.2. The coarse and fine stages are controlled by a Linux PC (Dell, XPS600, Pentium 4 3.80 GHz) through commercially available stage controllers (Sigma-Koki: Omec-4BG, Fine-503). The parallel link mechanism is controlled by the same PC through a D/A board (Contec DA16-16(LPCI)L) and a drive amplifier (MATSUSADA, HJPZ-0.15Px3). Displacements are measured with a strain gauge attached to piezoelectric devices and sent to a PC through a strain amplifier (Kyowa MCD-16A) and an A/D board (Contec AD16-16(PCI)EV) for PI control, in order to compensate for the hysteresis effect of the piezoactuator. Parallel mechanism control in a closed loop is shown in Fig. 3.3, and the duration of one control cycle is about 1 ms.

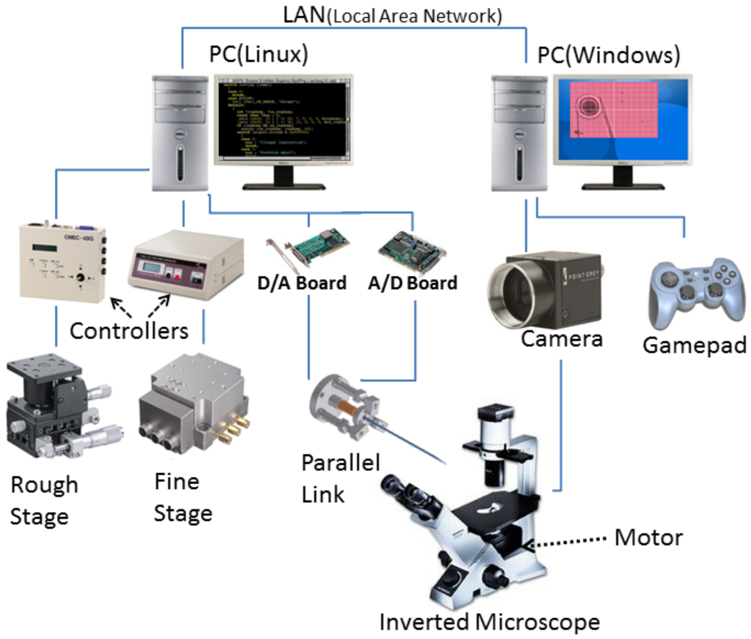
LAN(Local Area Network)
PC(Linux)
PC(Windows)
D/A Board
A/D Board
Controllers
Camera
Gamepad
Rough Stage
Fine Stage
Parallel Link
Motor
Inverted Microscope

Figure 3.1: System configuration.

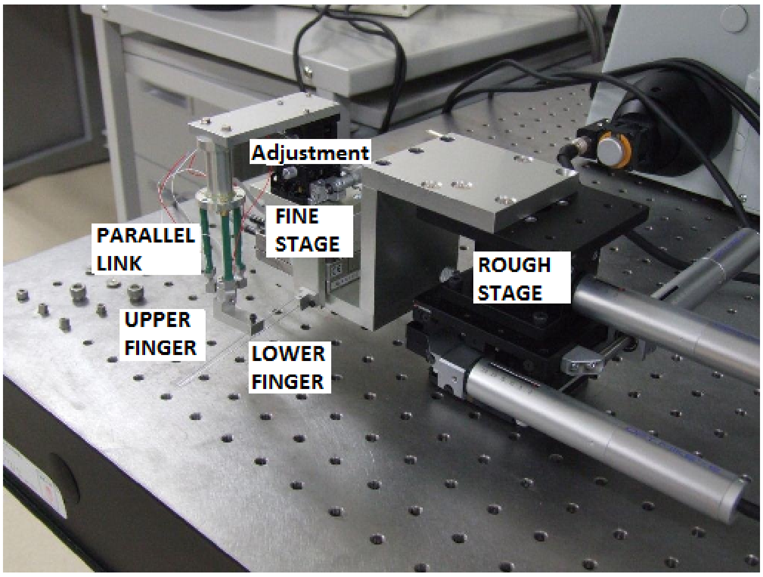
Adjustment
PARALLEL LINK
FINE STAGE
ROUGH STAGE
UPPER FINGER
LOWER FINGER

Figure 3.2: Micromanipulator prototype.

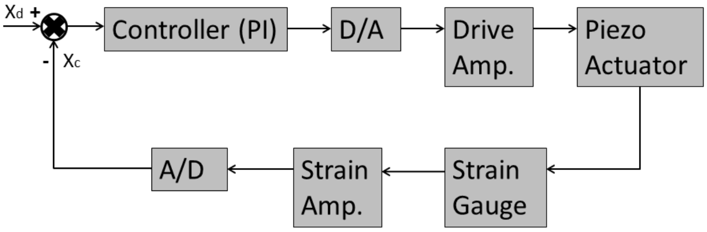

Figure 3.3: Parallel mechanism control.

The microhand and the target object are placed on the optical microscope stage. Images of end-effector ends are captured by the CCD camera (Point Gray Research, Flea) and displayed on a Windows PC. The motor on the microscope controls the motion of the objective lens, used in keeping the target object in focus manually. The end effectors, –the upper and lower fingers– of this micromanipulator consist of two glass needles that have a 1 mm diameter and sharpened ends with less than 1 μm in curvature. These needles are attached to the manipulator so that they can be replaced easily with new ones if they break, become worn, or are dirty.

As discussed in [69], a joystick is more efficient than a keyboard for micromanipulation tasks. Teleoperation between the user and the micromanipulator was therefore realized by using a joystick. We controlled the lower and upper modules, which consist of two motorized stages and the parallel link part, simultaneously with a cordless Gamepad (Logitech Rumblepad2).

The parallel link consists of three piezoactuators parallel to each other. An end effector is placed at the end of the parallel link. To control upper module movement accurately, the relationship between the parallel link extension through the strain gauge and the end effector position change through the camera was investigated. The parallel link mechanism was calibrated by obtaining the components of the calibration matrix that characterize the linear relationship between the displacement of the three piezoactuators and the change in the finger position in three directions. After calibration, absolute positioning accuracy is 2.1[μm] for the 132 μm range in the X and Y directions. Average error is 0.9 μm and standard deviation is 0.7 μm.

In this microhand system, the grasping and release of microobjects can be realized by teleoperation through the parallel link mechanism, where the transportation of microobjects is achieved both by teleoperation and by automating through coarse and fine stages.

3.1.2 Realization of Multi-Scalability

The purpose of the lower module is to achieve long-distance transportation of microobjects with precise positioning. As the coarse motion stage has large workspace with low accuracy and the fine motion stage has small workspace with high resolution, a combination of these two functions in the same system, which is the conventional coarse-to-fine motion strategy, offers the key to achieve the purpose of the lower module [42, 43]. Because the conventional method has a time delay between coarse and fine motions, however, we propose a coarse-to-fine motion strategy without time lag.

3.1.2.1 Conventional Coarse-to-Fine Motion Strategy

The conventional coarse-to-fine motion strategy is employed to improve positioning accuracy. The strategy procedure is as follows: target position (Xt) in the visible area of the microscope camera of the end effector is decided by the user. The system then sends the target position to the coarse motion stage and the end effector, which holds the microobject, moves to reach the target on the X-Y plane. Image resolution (Xr) depends on the magnification of the objective lens. By using a 60X objective lens, image resolution is 0.08 μm. The system should wait until the coarse stage finishes its motion by checking the current (Xc) and previous (Xp) positions of end effectors through template matching (3.1). Because the orientation of the end effector does not change during manipulation, we apply the template matching method.

$$\begin{aligned} &If: |Xc - Xp| \quad \geq Xr \quad coarse\ motion\ continues \\ &Otherwise: \qquad\qquad coarse\ stage\ stops \end{aligned} \tag{3.1}$$

When the difference between current and previous positions is smaller than Xr, which means the coarse motion stage has stopped, the system compares the target and current positions of the end effector through template matching. If the difference between them is less than Xr, the target position has been reached. If the difference is more than or equal to Xr, the difference is sent to the fine stage automatically to be compensated for (3.2).

$$\begin{aligned} &If: |Xt - Xc| \quad < Xr \quad motion\ is\ completed \\ &Otherwise: \qquad\qquad compensate\ the\ error \end{aligned} \tag{3.2}$$

Last, the fine motion stage finely aligns the microobject with the target position on the X-Y plane with 0.1 μm error. The precision of template matching is 0.08 μm and maximum error of the fine motion stage is 0.1 μm, meaning that 17 μm error of the coarse motion stage is minimized to 0.18 μm with the conventional coarse-to-fine motion strategy. The algorithm is summarized in the part including time lag in Fig. 3.4 at left.

3.1.2.2 Proposed Coarse-to-Fine Motion Strategy

Although large workspace with precise motion has been achieved using the above strategy, to decrease the duration of the transportation task, the strategy has been improved

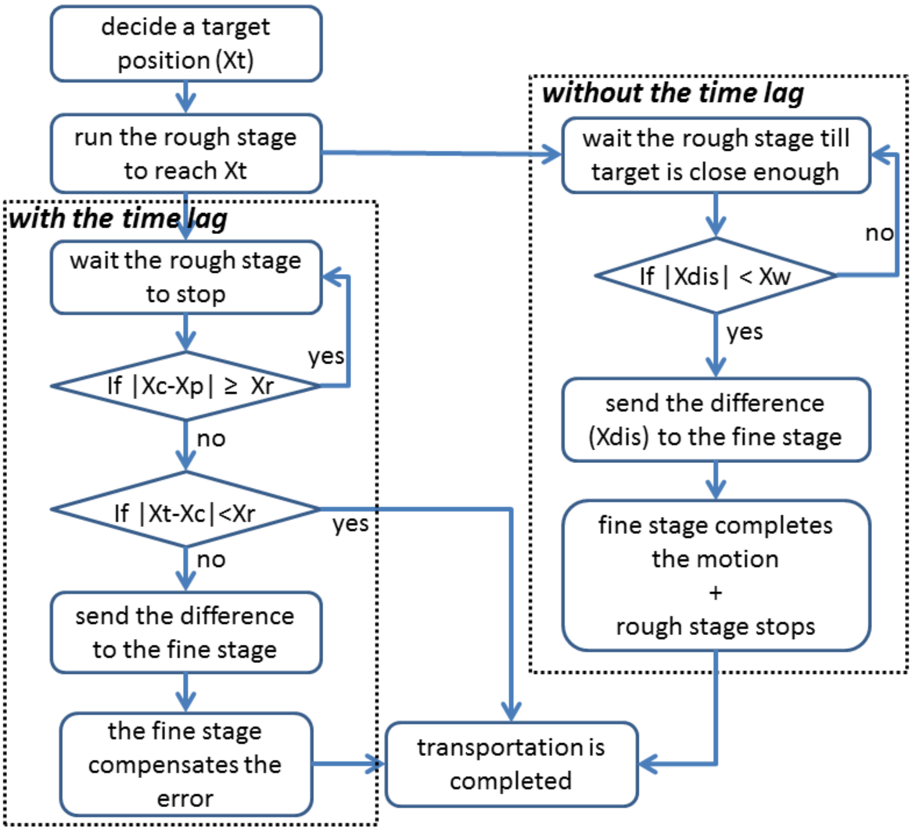
decide a target position (Xt)
run the rough stage to reach Xt
with the time lag
wait the rough stage to stop
If |Xc-Xp| ≥ Xr
yes
no
If |Xt-Xc|<Xr
yes
no
send the difference to the fine stage
the fine stage compensates the error
transportation is completed
without the time lag
wait the rough stage till target is close enough
If |Xdis| < Xw
no
yes
send the difference (Xdis) to the fine stage
fine stage completes the motion
+
rough stage stops

Figure 3.4: Accurate positioning flowchart.

by considering time lag.

As seen in the part that does not include time lag in Fig. 3.4, the system does not wait for the coarse motion stage to stop before compensating for error. When distance (Xdis) between the end effector and the target position is close enough, i.e., in the range of workspace for fine motion stage (Xw), which should be 50 μm, the system sends distance (Xdis) to the fine stage (3.3)-(3.4).

$$Xdis = Xt - Xc \tag{3.3}$$

$$\begin{aligned} If: |Xdis| &\geq Xw \quad coarse\ motion\ continues \\ Otherwise: &\qquad fine\ motion\ starts \end{aligned} \tag{3.4}$$

The fine stage moves the end effector to the target position. When fine motion starts, the coarse stage stops. Because the coarse stage cannot stop suddenly, motion between the stop command and completly stopping the coarse stage is considered when distance information is sent to the fine stage. When the fine stage finishes its motion, the transportation task is then completed with maximum error of 0.18 μm.

Conventional and proposed strategies are compared in Fig. 3.5. For the 150 μm travel distance in the X direction, the system needs 2.76 seconds for coarse motion, 1.31 seconds for time lag, and 0.005 seconds for fine motion, i.e., 4.08 seconds in total, to complete transportation with high precision (Fig. 3.5 (left)). Using the proposed strategy, in contrast, the system needs only 1.74 seconds to complete the transportation task as shown in Fig. 3.5 (right). Because the time lag depends on the system itself, e.g., the duration of communication between devices, even if the time lag is further shortened, our proposed strategy is still faster. With the first strategy, furthermore, the fine stage moves for a small distance, while with the second strategy, the fine stage moves for half of its workspace. Even if maximum error for both cases is 0.18 μm,

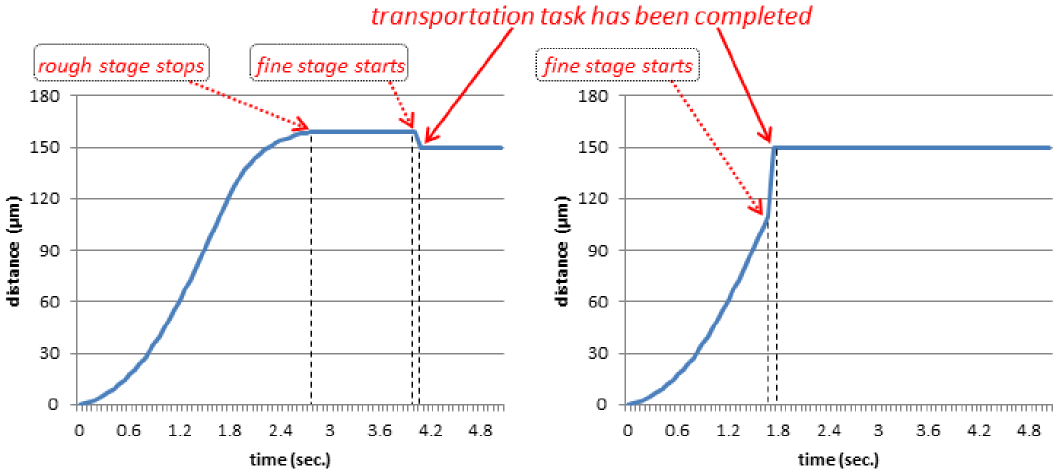

Figure 3.5: Comparison of conventional (left) and proposed (right) coarse-to-fine motion strategies.

error is therefore less for the first strategy most of the time.

As shown in Fig. 3.4, there are two routines for the system to continue: with and without the time lag. The user decides which routine is appropriate for the system with respect to priority such as time duration, speed, or accuracy.

From the beginning of manipulation, the system's end effector and target objects are placed on the same Z focal plane manually with the help of the motorized stage. Vision feedback strategy is used for manipulator positioning in 2D. If automatic control in the Z direction is necessary, however, we can extend our strategy to 3D by applying the All-In-Focus method [32].

3.2 Evaluation of Multi-Scalability

3.2.1 Experimental Results

The three experiments carried out with this system had the common feature that they used multi-scalability. First, various-sized microspheres were manipulated to show the ability of the system to manipulate multisized objects. Second, a cell fusion task was realized by manipulating donor and egg cells in the same scene. Third, extremely small and extremely large microbeads were manipulated in the same scene to show the precise positioning ability of the system, along with multisized object manipulability.

3.2.1.1 Manipulation of Various-Sized Microobjects

Microspheres, with diameters of 97, 55, 20, and 9.7 μm are manipulated to show that different-sized objects can be manipulated with this microhand. The entire process is realized in liquid on a glass and observed by 20x and 40x objective lenses. Fig. 3.6 shows the manipulation process for a 20 μm microsphere. Fig.3.6(a) and (b) show the grasping task, which includes moving both fingers to bring them close enough to the target object and moving the right finger to hold the target. Fig. 3.6(c) and (d) show a transportation task over a distance of 60 μm. Fig. 3.6(e) and (f) show a release task that includes moving the right finger and then moving both fingers away from the target object. This experiment was conducted as a predefined manipulation task via computer control. The entire manipulation process was the same for all target objects of different sizes. For each of the four different-sized target objects, the manipulation task was carried out 10 times to investigate the success of the process. Success of 100% for the grasping task (Fig. 3.6(a) and (b)), 100% success for the transportation task (Fig. 3.6(c) and (d)), and 80% success for the release task (Fig. 3.6(e) and (f)), were achieved after 40 trials.

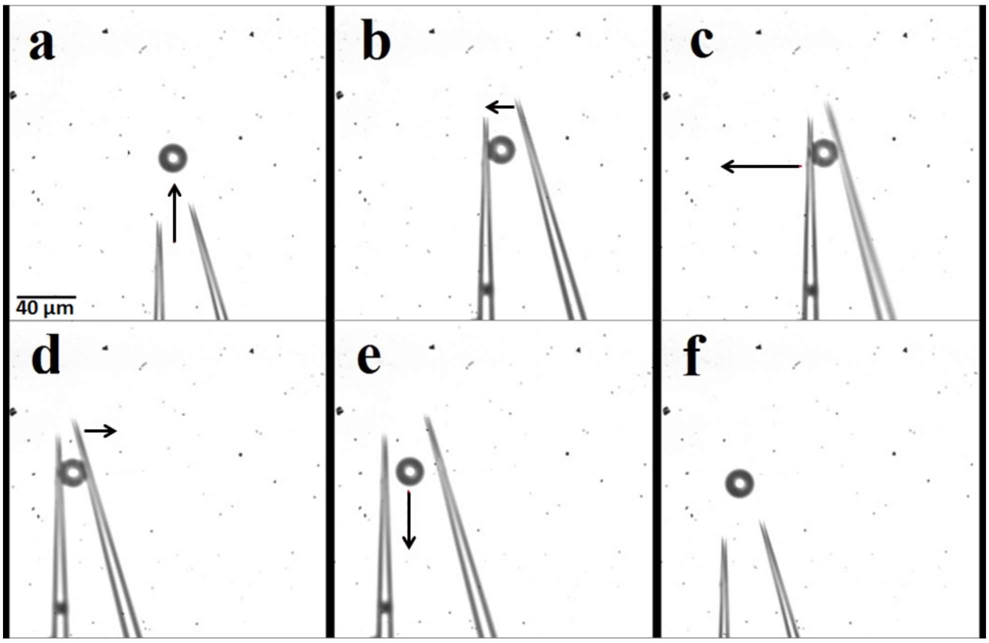

Figure 3.6: (a)-(b) Grasping task for 20 μm microspheres (c)-(d) transportation task for 60 μm distance (e)-(f) release process.

3.2.1.2 Cell Fusion Task

Cell fusion is one of the tasks possible for this micromanipulator in terms of multisized microobject manipulation. The procedure is as follows: a donor cell and an egg cell are placed under an optical microscope and the finger tips are moved using the stages until they are close enough to cells, then the microfingers hold, pick-up, transport, and release the different-sized cells, having them contact each other. The next stage of this task, which is the fusion of two cells with the help of an electrical current, is not performed here because the aim of this experiment is to investigate the capability of the system to be used in the manipulation of cells during a cell fusion task.

The handling of living cells is more difficult than that of microbeads. Because the duration of life for living cells in a normal environment is very short, cells are placed in a special liquid. In addition, living cells are stickier than microbeads, which makes the release task more difficult because adhesion is more effective on a micro-scale. We therefore prefer to release the cell by moving it to the end of the end effector, which has the smallest contact area compared to the rest of the end effector because adhesion between the tip of the finger and the grasped cell is the weakest. Furthermore, the target object is a soft living cell that poses no bending problem for the end effector. Donor cells, which are about 16 μm, and egg cells, which are about 100 μm, were used. We were able to successfully manipulate –hold, pick-up, transport, and release– the donor and egg cells in the same scene, as shown in Fig. 3.7 and to make them contact each other with the help of teleoperation. We thus say hence that cell fusion tasks can be performed with this system.

3.2.1.3 Multi-Scalability of the System

To show the system's multi-scale manipulability, extremely small and extremely large microbeads are manipulated in the same scene and observed with a 10X objective lens

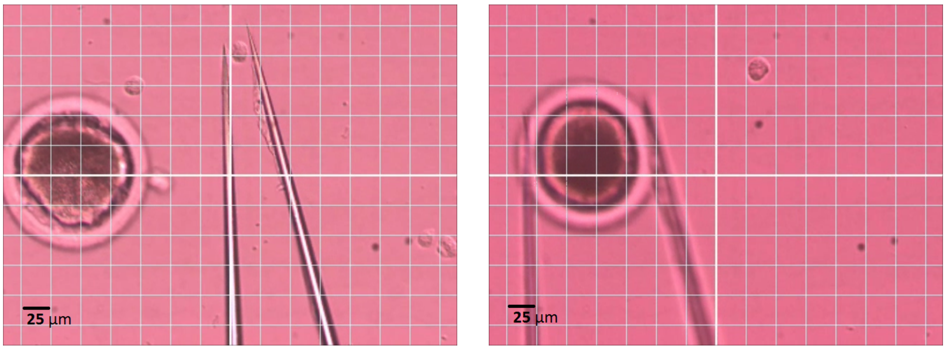

Figure 3.7: Manipulation of donor (left) and egg (right) cells.

as shown in Fig. 3.8.

The microhand grasps and transports a 115 μm microbead to the target position, which is the center of the screen, and releases it. Then, in the same situation, the microhand successfully manipulates an 8 μm microbead using a similar procedure. The entire process is conducted combining teleoperation for grasping and release tasks and the coarse-to-fine motion strategy for the automatic transportation task. Precise positioning with 0.15 μm error is achieved with the proposed strategy.

Because the resolution of the parallel mechanism is on the sub-micron level, the manipulation of smaller objects of about 1 μm can be realized with this system. Because finding the center of a 1 μm microbead is difficult and small objects are easily affected by liquid flow, however, it is extremely difficult to accurately grasp objects a few microns in size in liquid without a special strategy.

3.2.2 Discussion

The performance of the developed system is shown in Table 3.1, and a comparison of multisized objects manipulability with similar studies is shown in Table 3.2. In

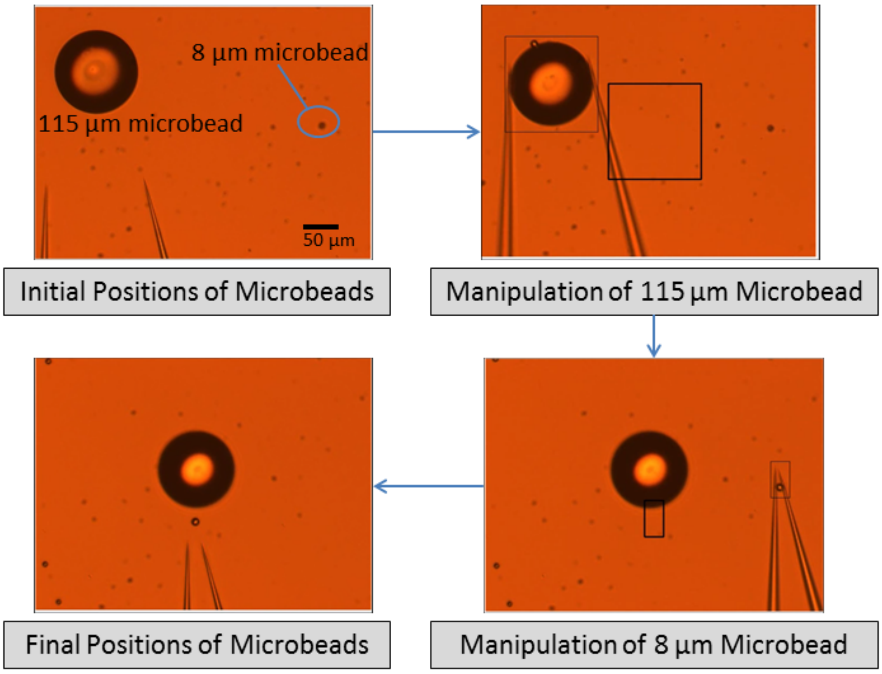
8 µm microbead
115 µm microbead
50 µm
Initial Positions of Microbeads
Manipulation of 115 µm Microbead
Manipulation of 8 µm Microbead
Final Positions of Microbeads

Figure 3.8: Realization of the system's multi-scalability.

Table 3.1: Micromanipulator performance

	global motion	local motion
workspace (mm)	25.1x25.1x10.1	0.13x0.04x0.02
max. speed (mm/sec)	1.7 (distance$\leq$0.1mm) 0.1 (distance$>$0.1mm)	110
observable resolution (μm)	0.1	0.1
accuracy (μm)	0.18	2.1
repetability (μm)	0.15	2.5

Table 3.2: Comparison to similar manipulation systems

	mh(1)	mh(2)	mh(3)
multisized objects manipulability (μm)	3-17	20-100	1-132

similar studies, the manipulation of microobjects was realized by different types of microhands that we call microhand (1) [28] and microhand (2) [41]. These two similar studies were chosen for their multi-scalability and similar target objects. As shown in Table 3.2, the manipulability of multisized objects achieved by our proposed system, called microhand (3), is better than that of the studies compared.

Our micromanipulation system can be used to manipulate various-sized microobjects from 1 μm to 132 μm. If the target object size, e.g., tissues, is more than 132 μm, however, this system cannot be used and further improvement of workspace size is necessary. This system is by no means the final multi-scalable system and its multi-scalability can be further improved to realize a general-purpose microhand.

4

Vibration Control for Stable Grasping at High Speed

4.1 Introduction

To construct a multi-layered cell assembly, it is essential to achieve the pick-and-place of single-cell using a two-fingered micromanipulation system. The first step towards this goal is realizing the high-speed grasping of the cells. High speed is a necessary requirement for such a micromanipulation system because of the presence of a vast number of cells and their restricted life span.

In this chapter, a two-fingered microhand (Fig. 4.1) for high-speed cell handling is studied. Rapid point-to-point movements for the end effector of the robot are involved in the pick-and-place task. To grasp a cell quickly, the end effector of the microhand needs to move towards the cell. This motion involves accelerating of the end effector to a required operational speed and decelerating to a full stop. The abrupt changes in acceleration or deceleration often result in residual vibration. When the grasping motion is carried out at high speed, the residual vibration has a greater impact on the process. It may cause location change of the target cell, damage it and lead to a long

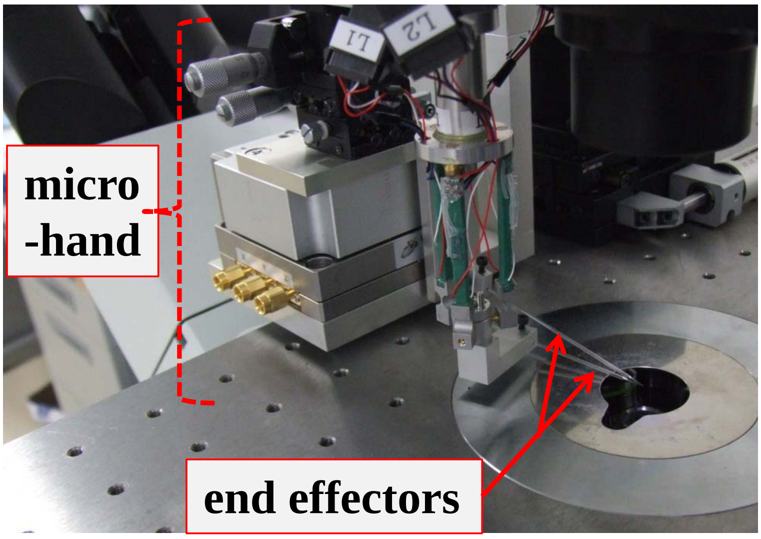

Figure 4.1: The microhand with the end effectors.

settling time of the system.

To realize successful grasping of microobjects at high speed, it is necessary to analyze the vibration behavior and develop an efficient suppression method. Tao et al. modeled the residual vibration and used an acceleration smoother to suppress the vibration of the SCARA robot arm [64]. In the microrobotics field, most of the studies focus on the vibration suppression of piezo actuators, as the oscillation is the natural result of applying voltage to the piezo material [65–68]. However, the residual vibration suppression in a microhand has not been studied yet.

There are a few existing approaches which can be applied to suppressing the vibration of the end effector of the microhand :

- Increasing stiffness of the system by structural design to increase damping [70, 71].
- Trajectory smoothing to achieve smooth acceleration and deceleration [72–74].

- Input shaping to cancel the system's own vibration [75, 76].
- Feedforward control [77].
- Feedback control [78, 79].

To achieve an effective damping in the system, we increase the stiffness of the microhand by increasing the thickness of the end effectors. To further decrease the residual vibration, we need to apply an appropriate control method. As we can predict the behavior of the vibration (frequency, amplitude, settling time, etc.) for a specific acceleration, we can implement the feedforward control to suppress the vibration in the system.

The structure of the paper is as follows. In section 4.2, the microhand system is described and the residual vibration of its end effector is explained. The vibration of the end effectors of the microhand is analyzed in section 4.3. Finally, in section 4.4, the vibration suppression through structural design and the feedforward control is presented. In addition, the experimental results are discussed.

4.2 Micromanipulation System

The experimental setup for the micromanipulation at high speed is shown in Fig. 4.2. In this system, the main part is a two-fingered microhand. The microhand is composed of two main parts: a lower and an upper module. Details of those modules can be found in section 2.1.

The coarse and fine stages are controlled by a Linux PC (Dell, XPS600, Pentium 4 3.80 GHz) through commercially available stage controllers (Sigma-Koki: Omec-4BG, Fine-503). The parallel link mechanism is controlled by the same PC through

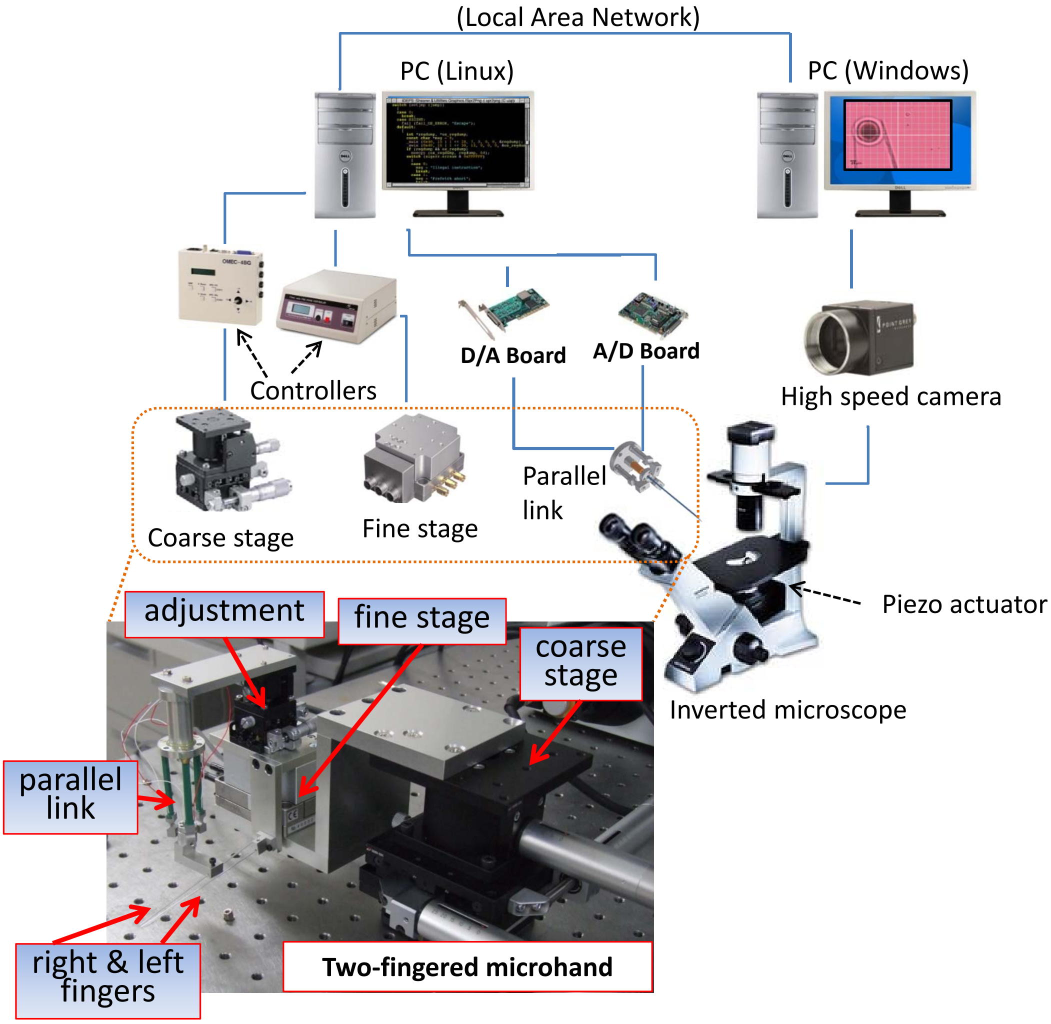
(Local Area Network)
PC (Linux)
PC (Windows)
D/A Board
A/D Board
Controllers
High speed camera
Coarse stage
Fine stage
Parallel link
Piezo actuator
Inverted microscope
adjustment
fine stage
coarse stage
parallel link
right & left fingers
Two-fingered microhand

Figure 4.2: System configuration.

a D/A board (Contec DA16-16(LPCI)L) and a drive amplifier (MATSUSADA, HJPZ-0.15Px3). The displacements are measured with a strain gauge attached to the piezoelectric devices, and sent to the PC through a strain amplifier (Kyowa MCD-16A) and an A/D board (Contec AD16-16(PCI)EV) for PI control, in order to compensate the hysteresis effect of the piezo actuator. This closed-loop control of the parallel mechanism is shown in Fig. 3.3 and the duration of one control cycle is about 0.35 ms.

The two end effectors of the microhand and the target object are observed under an IX81 motorized inverted optical microscope using an Olympus LUCPlanFLN 20x/0.45na Ph1 objective lens. The images are captured with a high-speed camera (Photron FASTCAM MC2) and displayed on a Windows PC (Intel Core i7 CPU, 2.93GHz with 4 GB RAM) monitor. The end effectors - the right and left fingers - of this micromanipulator are glass needles which have a 1 mm diameter and sharpened ends with a curvature of less than 1 μm. While the left end effector is connected to the lower module, the right end effector is mounted onto upper module. In total, the microhand can therefore perform movements in a large workspace (coarse stage) with high precision (fine stage), and grab, rotate and release objects by the relative movement of the right end effector (parallel link).

The maximum speed of the microhand is 2.3 mm/s. As the feasible maximum speed of the actuators depends on the applied voltage and the features of the actuator itself, higher speed can be realized with other actuators.

When the stage runs at normal speed (0.1 mm/s), there is no effective vibration for most of the microhand systems. To grasp a cell quickly, however, the end effector of the microhand needs to move towards the cell at high speed. This motion involves accelerating to required operational speed and decelerating to a full stop. The abrupt changes in acceleration or deceleration often result in residual vibration. When the grasping motion is carried out at high speed ($\geq$ 1 mm/s), the residual vibration is greater which may cause dropping and even damaging a cell during transportation. In addition, the settling time is longer, which is not a desirable feature in the high-speed grasping of the microobjects. Therefore, to realize an appropriate vibration control method, we carried out the vibration analysis in the microhand [80].

4.3 Vibration Analysis in the Microhand

4.3.1 Oscillation Observation

The oscillations of the end effectors during and after the motion were recorded with a high-speed camera. The camera was set to capture images at 2000 frames per second with a magnification of 20X (252 x 252 μm^2 image size and 1 pixel = 0.494 μm). With this configuration, the oscillation could be easily observed. The magnitude and the relation to the moving direction (perpendicular or parallel to the end effectors) could be identified roughly and directly from the captured images.

For more accurate and faster handling of big image batches, the end effector position is saved to be used in image processing. With image processing, the contours of the end effectors are detected based on the difference in brightness between the background and the end effector. The coordinates of the end effector tip are determined as follows. The topmost pixel of the contour corresponds to the y coordinate. Calculating the centroid of the contour and assuming a constant angular orientation of the end effector, the x coordinate can be derived, as seen in Fig. 4.3. This algorithm can be applied to the image batches saved beforehand.

To analyze the vibration of the system, the fine stage moves with the speed of 2.3 mm/second for 80 μm. An exemplary plotted result of the oscillation is given in Fig. 4.4. The vibration during the motion is small. The residual vibration after the motion is great however. Looking at the magnitudes of the oscillations, we can say that the right end effector oscillates with higher magnitudes (up to 29.1 μm) than the left one (5.76 μm). Furthermore, the oscillation in the y-direction is smaller than the one in

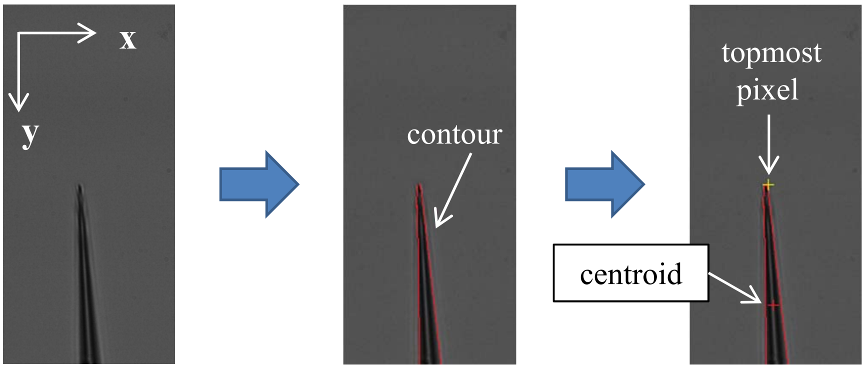

Figure 4.3: Position detection that is showing the contour, centroid and end effector tip.

the x-direction. Since objects are grabbed and held by the relative movement and force in the x-direction, vibration control with the aim of removing the oscillations in the x-direction was prioritized.

4.3.2 Frequency Analysis of Oscillation

As Discrete Fourier Transform (DFT) takes a discrete signal in the time domain and transforms it into its discrete frequency domain representation, the DFT is an appropriate method for frequency (spectrum) analysis. Let χ_0, ..., χ_{N-1} be complex numbers. The DFT is defined by the formula:

$$X_k = \sum_{n=0}^{N-1} \chi_n e^{-i2\pi k \frac{n}{N}} \quad k = 0, ..., N-1. \tag{4.1}$$

A Fast Fourier Transformation (FFT) computes the DFT and produces exactly the same result as when evaluating the DFT definition directly; the only difference is that an FFT is much faster.

The data sets (obtained from image processing) were analyzed using the FFT. The objective of this analysis was to determine the frequencies occurring within the end effector oscillations. This analysis provides information about the nature and cause of

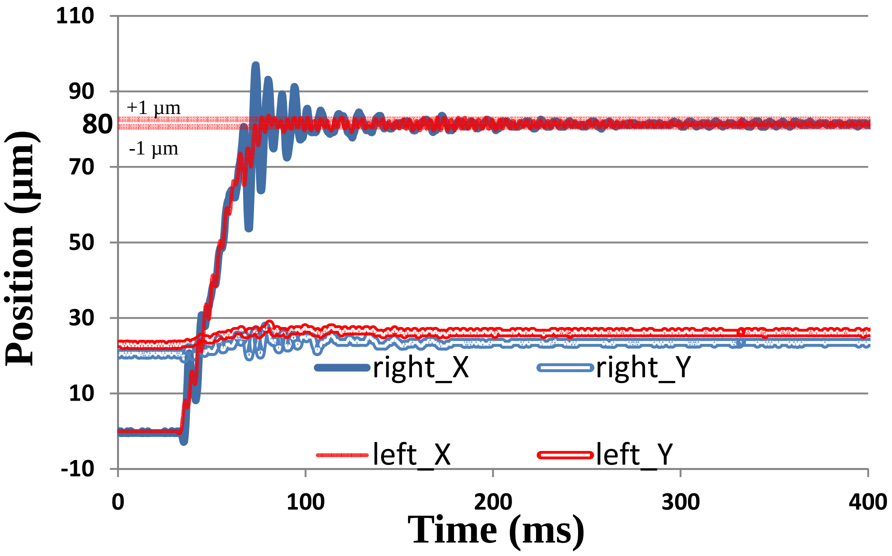

Figure 4.4: Oscillation of both end effectors in x and y caused by 80 μm motion.

the vibration. In addition, it shows the highest present frequency.

The FFT analysis shows that the frequency spectra of the left and right end effectors are quite different, as shown in Fig. 4.5. The left end effector oscillates with but a single –its natural– frequency (170 Hz). The right end effector sways with the superposed frequencies. The highest occurring frequency is the right end effector's natural frequency, at about 260 Hz.

4.4 Vibration Suppression of the End effectors

4.4.1 Structural Design to Increase Damping

To increase the damping of the system, the thickness and mass of the fingers were considered. Equation (4.2) shows that a heavier finger has a lower natural frequency (F_n).

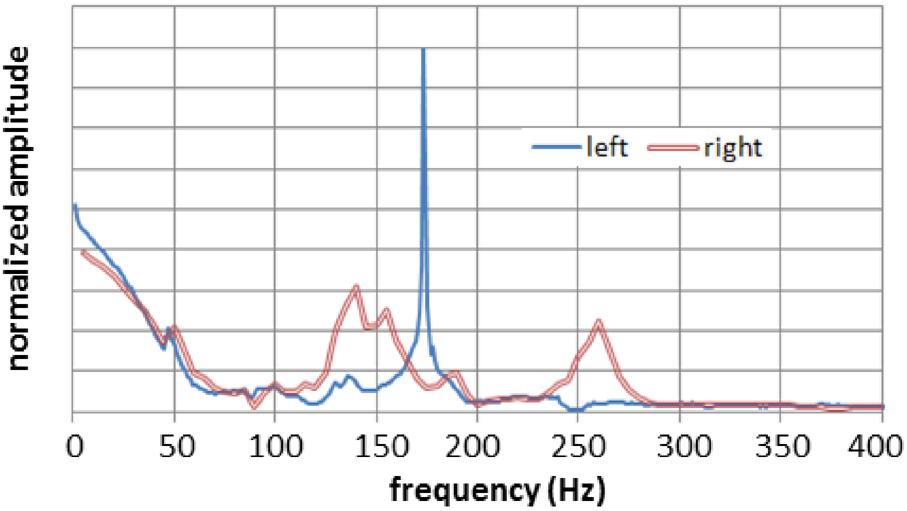

Figure 4.5: Result of Fast Fourier Transform of x position of the left and right end effectors.

$$F_n \propto \sqrt{\frac{EI}{mL^4}}. \tag{4.2}$$

E stands for elastic modules, while I stands for the moment of inertia; m represents the mass of weight, and L is the length of the end effector. Moreover, a thicker finger oscillates with a considerably smaller magnitude (4.3) where δ_{max} represents the maximum deflection and w stands for applied force.

$$\delta_{max} \propto \frac{wL^4}{EI}. \tag{4.3}$$

With respect to the dynamics theory of a beam under uniform load, the microhand was redesigned by increasing the thickness (4 times) and the mass (3 times) of the end effector's holders by considering structure of microhand system as shown in Fig. 4.6. For the left end effector, the amplitude of the oscillation was decreased to the imperceptible level (max. deflection $\approx$1 μm with a settling time of 20 ms). On the other

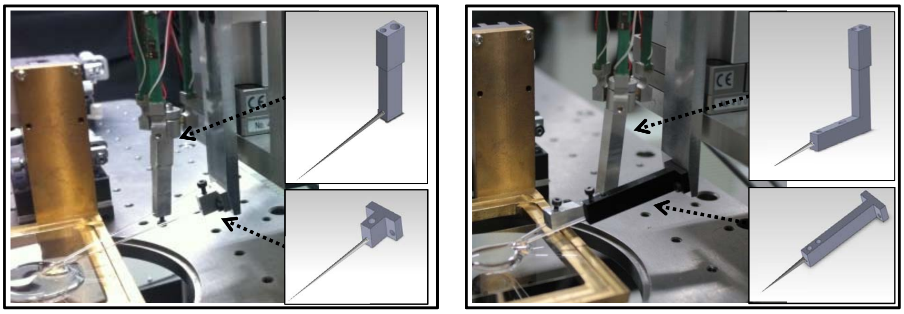

Figure 4.6: End effectors before (left) and after (right) structure modification.

hand, for the right end effector, the vibration was still great (max. deflection: 25.88 μm, settling time: 173 ms) as illustrated in Fig. 4.7. The settling time is the time taken from motion completion time to the time when the end effector vibration fall within a fixed threshold (set to $\pm$ 1 μm in our experiments). The natural frequency of the right end effector is 60 Hz as shown in Fig. 4.8. The parallel link mechanism, moving the right end effector, has very thin and long spherical joints, which are the main cause of the vibration.

Seeing the differences in magnitude as well as in the means of actuation (the right end effector can be actuated relatively to the global motion of the hand), we decided to work on the right end effector. The residual vibration control of the right end effector is discussed in the next section.

4.4.2 Residual Vibration Control of the Right End Effector

To decrease the residual vibration further, we need to apply an appropriate control method. Trajectory smoothing and input shaping are not available approaches for the microhand system, as the signal can not be changed during the motion for the fine stage we use with a controller to move both end effectors. The velocity and the distance of the motion can be decided by the user but the signal to the controller can not be altered

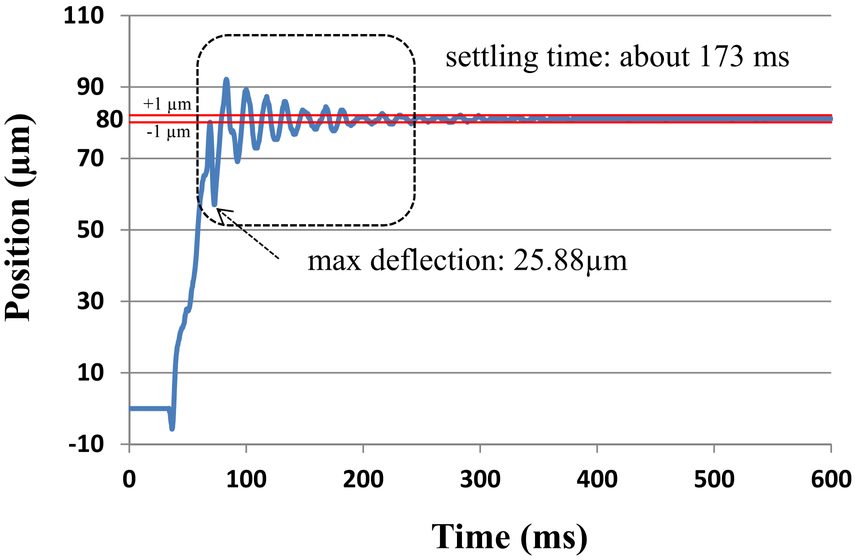

Figure 4.7: Vibration of right end effector after structure modification.

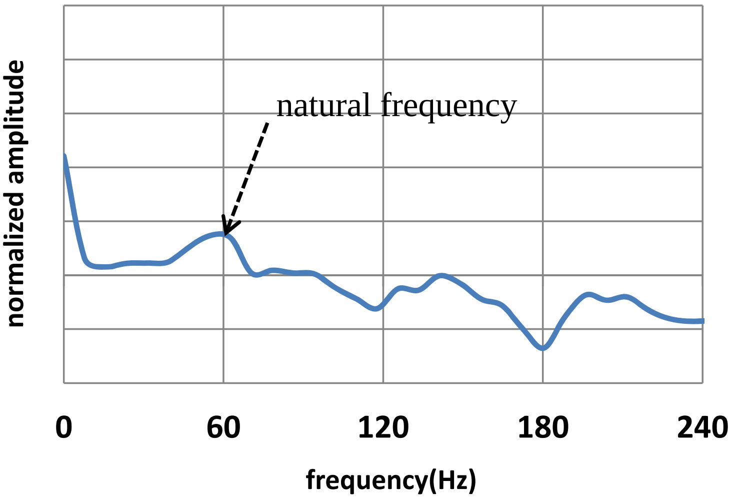

Figure 4.8: Vibration frequency of the right end effector is 60 Hz.

during the motion. Although the feedback method is a reliable way to control the vibration, the sampling time should be at least 10 times of the vibration frequency, which is not feasible for the current system. As we can predict the behavior of the vibration (frequency, amplitude, settling time, etc.) for a specific acceleration however, we can apply the feedforward control to decrease the residual vibration of the system.

4.4.2.1 Real Time Image Processing

To realize the vibration control in real time, the image processing can no longer be done on a batch of images saved beforehand. The finger position has to be determined directly after capturing an image. Therefore the processing time has to be decreased as much as possible.

The image width was constrained by defining a region of interest (ROI). By observing the oscillation (4.3.1), we learn that the finger moves less than the maximum distance between the two following frames. This distance depends on the frame rate and the lens used. A 20X magnification lens (1 pixel = 0.494 μm) was chosen to cover a big workspace of 252 x 252 μm^2. The ROI to be processed in the following frame is defined by adding this maximum distance to both sides of the current finger position. As a result, an image capturing and processing rate of 2000 Hz was realized.

Sometimes, the finger oscillates too strongly and will not be within the processed region (occurrence $< 1\%$). In this case, the ROI is reset to the center of the image in order to increase the chance of redetecting the finger in the next frame.

The controller output has to be sent to the computer commanding the parallel link mechanism. The connection between the two computers used was tested for possible sending rate and delay time. A sending rate of 2000 Hz with a transmission delay time of 0.5 ms was ascertained.

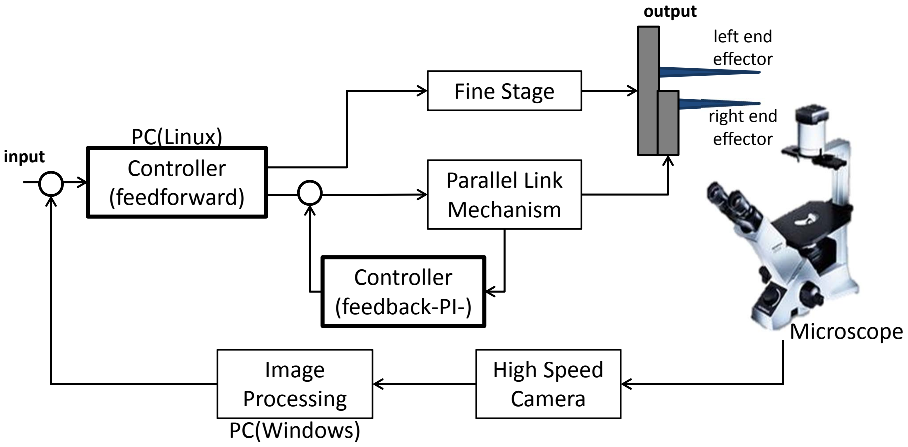
output
left end effector
right end effector
input
PC(Linux)
Controller (feedforward)
Fine Stage
Parallel Link Mechanism
Controller (feedback-PI-)
Microscope
Image Processing
PC(Windows)
High Speed Camera

Figure 4.9: Block diagram of the vibration control system.

4.4.2.2 Control Loop Design

Considering the control aims, the deviation between the actual and the target position is processed and fed back to the system. The difference is calculated on the Windows computer doing the image processing. The result is then sent to a second computer (Linux), responsible for moving the parallel link mechanism, as shown in Fig. 4.9. The two computers are connected via a regular LAN. The system has to be set up on two different computers, because the high-speed camera only provides a Windows driver, while some control tasks for the microhand require an ART-Linux computing system.

There are two levels of vibration control, as seen in Fig. 4.9. The first level is the feedback control (PI) of the parallel mechanism, meant to compensate hysteresis of the piezo actuators. However, we need to choose P and I gains very carefully so as not to produce any vibration of the piezo actuators. Results show that, while compensating hysteresis to avoid producing any vibration, P and I gains should be very small (P:0.3, I:0.1) which takes about 3 ms to complete parallel mechanism motion. Second level of vibration control is achieved with the feedforward method. The feedforward control starts according to image processing results. The parallel mechanism moves the right end effector to the opposite direction of the oscillation to control the residual vibration.

In summary, it can be stated that an image capturing, processing and error calculation rate of 2000 Hz is achieved. The delay time for sending the data to the Linux PC is 0.5 ms. Thus the entire control loop can be run at 1000 Hz. The delay between giving a command on the Linux PC and the parallel link executing the command is about 3 ms. In total, however, the entire delay time should add up to 4.0-4.5 ms.

4.4.2.3 Set-Point Determination

To control the vibration, the actual end effector position has to be compared to a set-point value. This is the value the control task aims to reach. The set-point for the control task once the global motion has ended is identical to the targeted position of the end effector. By converting the moving distance *d* into an amount of pixels and adding it to the initial position (pos_0), the coordinates of the destination (pos_{dest}) can be calculated (4.4).

$$\begin{aligned} pos_{dest} &= pos_0 + d/\lambda \\ where: \ [\lambda] &= \mu m/pixel \end{aligned} \tag{4.4}$$

The ratio λ depends on the lens in use. In the case of the 20X magnification, it is $\lambda = 0.494$.

4.4.2.4 Experimental Results and Discussion

The procedure of the high-speed grasping motion is as follows: First, the fine stage runs with 2.3 mm/second for 80 μm to make the end effectors approach to the target object quickly. When the end effectors reach the target position, the system informs the parallel mechanism in real time by visual feedback, in order to suppress the residual vibration. When the fine stage stops, the parallel mechanism moves the end effectors

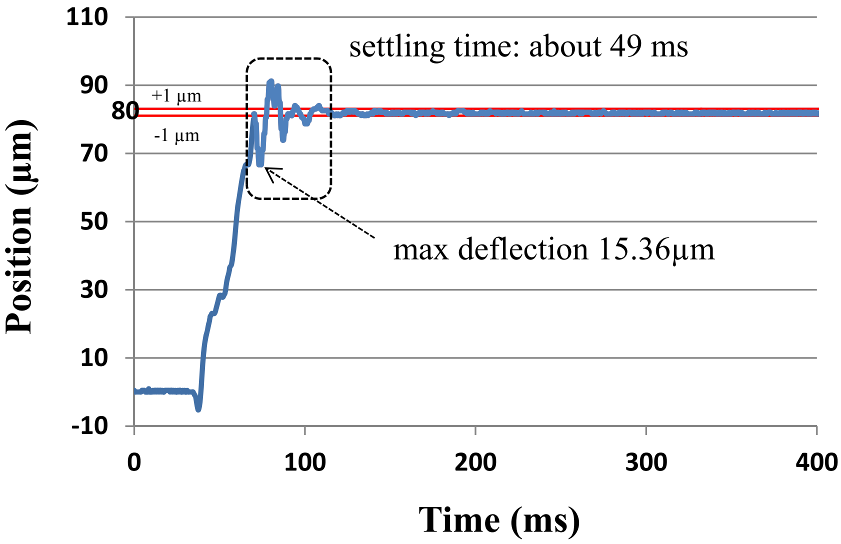

Figure 4.10: Vibration after compensation.

to the opposite direction of the residual vibration for a decided number of cycles using the feedforward control, in order to settle the oscillation. During the feedforward control, there is no sensory information used. With the feedforward control, the residual vibration of the right end effector is decreased. The settling time is 49 ms, with a maximum deflection of 15.36 μm, as seen in Fig. 4.10.

In brief, to achieve stable grasping at high speed, we analyze the vibration of the end effectors. Analysis results show that both end effectors show great oscillation at the end of the motion. To increase the damping of the system, we modify the structure of the end effectors. As a result, the amplitude and settling time of the vibration for the left end effector decrease to the imperceptible level, at which high-speed stable grasping is feasible. For the right end effector, the residual vibration is still great, however. Therefore, we apply the feedforward control to the right end effector and achieve a further decrease in the vibration, as illustrated in Table 4.1.

We can predict the exact model of the vibration based on the analysis results. Thus,

Table 4.1: Vibration and settling time after vibration suppression

	Left End Effector		Right End Effector	
	Deflection (μm)	Settling (ms)	Deflection (μm)	Settling (ms)
Original Values	5.76	226	29.1	192
Structural Design	1	20	25.88	173
Average Improvement (%)	83	91	12	10
Feedforward Control	-	-	15.36	49
Average Improvement (%)	-	-	47	74

we can say that the feedforward control is appropriate for the residual vibration problem. If there is any unexpected disturbance, e.g. vibrational motion of the microhand actuators on the platform, however, the resulted vibration can not be suppressed with the feedforward method. Consequently, to realize a more robust control of the vibration, the feedback method will be applied as a next task after achieving a sampling time of 10 times the vibration frequency.

5

Fast 3D Detection of Microobjects for High Speed Micromanipulation and Experimental Results

5.1 Materials and Methods

5.1.1 System Configuration

In this section, we introduce the experimental setup for high-speed micromanipulation. In this system, the main part is a two-fingered microhand. The microhand is composed of two main parts: a lower and an upper module. The lower module is for global motion, that is the movement of both end effectors. With global motion, the transportation of target objects and the positioning of the microhand can be achieved. Two motorized stages, the coarse (Sigma-Koki, TSD-805S) and the fine (Sigma-Koki, SFS-H60XYZ) stages form the lower module, and help realize the large workspace and precise motion necessary for the manipulation task. The specifications of the fine and coarse stages are listed in Table 2.1. Details can be seen in section 2.1 and 4.2.

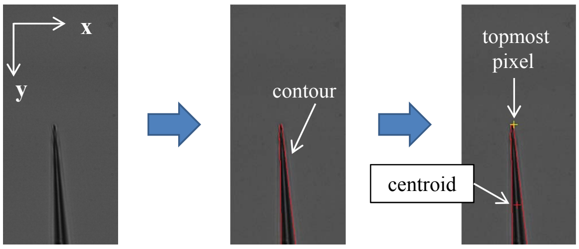

Figure 5.1: Detection of finger tip position.

5.1.2 High Speed 3D Position Detection

In this research, a top-down scanning of the target microobject and microfingers is performed by using a piezo actuator that can move the objective lens over a distance of up to 100 μm along the optical axis at 15 Hz. Although the working range of the piezo actuator is 100 μm, it was set to 90 μm, in order to avoid a strong vibration being induced when the actuator reaches the upper and lower extremes at high speed. The actuator moves the objective lens with a 1 μm step, while the high-speed camera captures the image at 2,000 frames per second. A stack of 90 images captured at consecutive and equally spaced focal planes is thus obtained. By searching for the index of the image in which the target object or the microfinger is best focused, its z-position is obtained.

5.1.2.1 Microfinger detection

The best focused image of the microfinger is searched in the stack of 90 images by template matching. In order to reduce the computation time for template matching, a region of interest in the image is defined automatically. Since the microfingers are within the scanning range of 90 μm in z-space, they are out of focus in a few images located in the topmost positions in the image stack. Precise detection of the 2D position is not feasible from these topmost images; however, the image region of the defocused microfinger can be defined.

Due to the constant orientation of the microfinger and its unique elongated shape in the image, the region of interest for finding the z-position of the microfinger by template matching is defined by the following process:

- Binary thresholding of the image, followed by contour calculation;
- Detection of the contour of the microfinger based on its elongated orientation;
- Detection of the microfinger tip (x_{tip}, y_{tip}) as the topmost point of the microfinger contour (see Fig. 5.1);
- Defining the region of interest of 100 × 140 pixels for template matching. The top-left coordinate of this region is $(x_{tip} - 20, y_{tip} - 20)$.

With the region of interest of each image in the image stack, template matching is performed to search for the focused image of the microfinger. The size of the template image is 60 × 100 pixels; the normalized correlation coefficient matching method is used. The best correlation coefficient is recorded for each image in the image stack and the best focused image corresponds to the image with the largest normalized correlation coefficient. Since images in the stack are captured continuously during the top-down scanning with a 1 μm step distance, the index k of the best focused image corresponds to position $z = 90 - k$, where $1 \leq k \leq 90$.

5.1.2.2 Object detection

In this research, the best focused image of the target microobject is found by applying our novel autofocus algorithm that analyzes the intensity variation at the outer region of the object border in the frequency domain. The proposed autofocus algorithm is called “Depth from border intensity variation” [81].

For every image in the image stack, the algorithm starts with the detection of the target object in the image, by performing binary thresholding on the image and finding

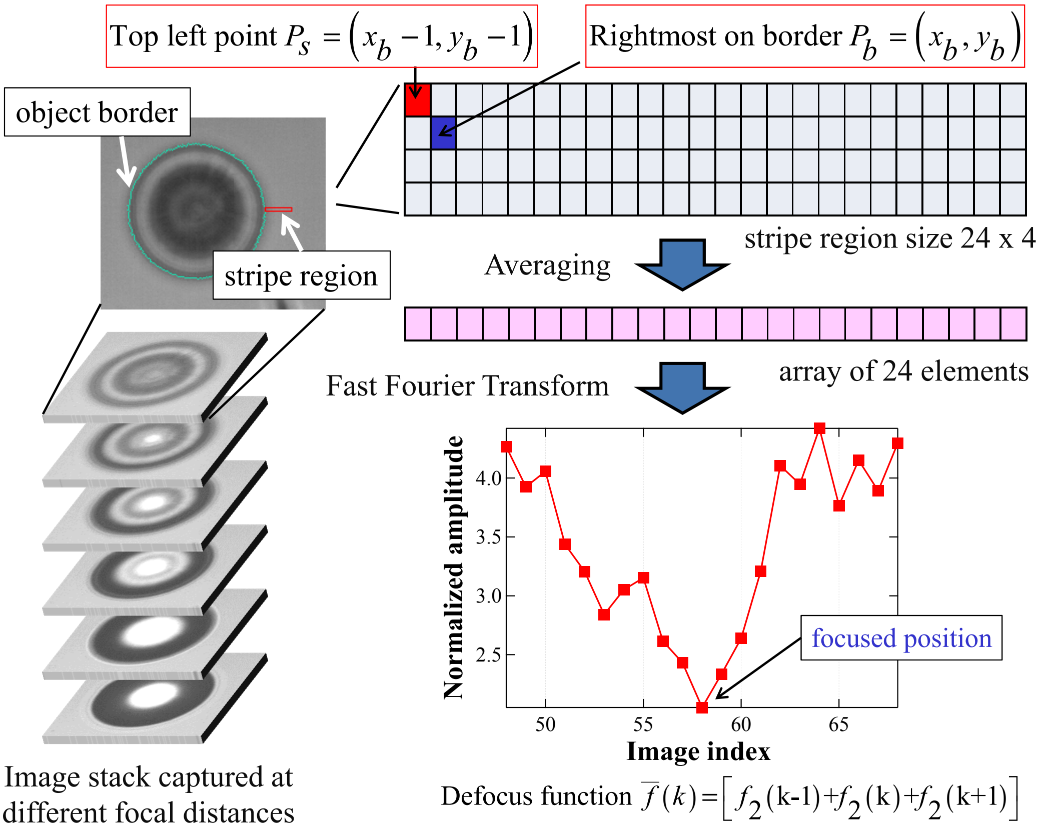
Top left point $P_s = (x_b - 1, y_b - 1)$
Rightmost on border $P_b = (x_b, y_b)$
object border
stripe region
stripe region size 24 x 4
Averaging
array of 24 elements
Fast Fourier Transform
Normalized amplitude
4.0
3.5
3.0
2.5
50
55
60
65
Image index
focused position
Image stack captured at different focal distances
Defocus function $\overline{f}(k) = [f_2(k\text{-}1) + f_2(k) + f_2(k+1)]$

Figure 5.2: Depth from border intensity variation algorithm.

the object contour. In this research, microspheres are used as target microobjects. They can be detected as circular contours. After the object contour is obtained, the rightmost point $P_b(x_b, y_b)$ on the contour is used to define a stripe region of 24 × 4 pixels. The top-left point of the stripe region is defined as

$$P_s(x_s, y_s) = (x_b - 1, y_b - 1) \tag{5.1}$$

This definition of P_s is used to compensate for inaccurate border detection and to filter out image noise. By averaging the values of pixels having the same y-coordinate in the stripe region, an array of 24 intensity values along the stripe region in the x direction is obtained. The one-dimensional Fast Fourier Transform is then applied to this array. The Fourier spectra is normalized by the DC component, i.e., the average intensity of the stripe region, so that the Fourier spectra obtained from other images can be compared.

Let f_2 be the second frequency of the Fourier spectrum. The defocus function is defined from f_2 as:

$$\bar{f}(k) = [f_2(k-1) + f_2(k) + f_2(k+1)]/3 \tag{5.2}$$

Where k is the index of the image in the stack and $0 < k < 89$.

The defocus function can be considered a filtered version of f_2, to minimize the fluctuation of f_2. The autofocus algorithm searches for the minimum position of $\bar{f}(k)$, which corresponds to the best focused image of the microsphere (see Fig. 5.2). A detailed explanation of this algorithm can be found in the relevant section in [81].

To evaluate the robustness of the detection algorithm, autopositioning experiments are carried out (Fig. 5.3). The process of autopositioning includes measuring 3D positions of both end effectors and target microobjects and autofocusing to the object, followed by z-alignment of the end effectors and target objects, i.e., moving the end effectors to the same z-level as the target object (Figs. 5.4a–c). Autopositioning is

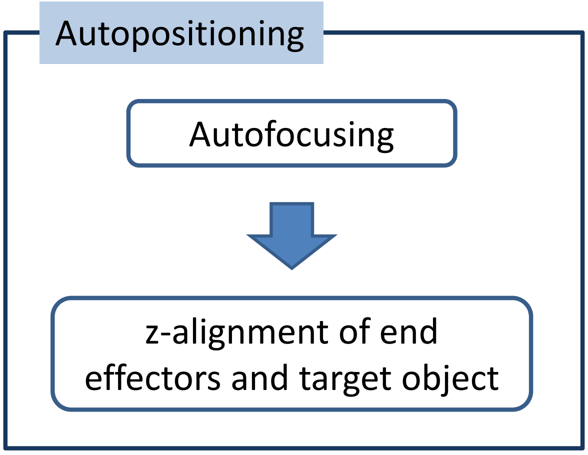

Figure 5.3: Flow chart of high speed autopositioning.

considered successful if the end effectors can grasp the center of the target object in the manipulation process. Autopositioning process takes about 340 ms, with a success rate of 74% (74 out of 100 trials). To improve the robustness of the detection method, we propose the following modification in the detection algorithm.

Replacement of binary thresholding: When we have to deal with a dynamic environment, there are many factors that can easily cause a system to fail. In our case, the effect of lighting is crucial. It sometimes leads to false recognition, as the traditional binary thresholding method considers the overall image brightness. Therefore, we replaced the binary thresholding with adaptive methods. The adaptive threshold module is usually used in uneven lighting conditions when we need to separate a lighter foreground object from its background. It performs binary thresholding by analyzing each pixel with respect to its local neighborhood. This localization allows each pixel to be considered in a more adaptive environment.

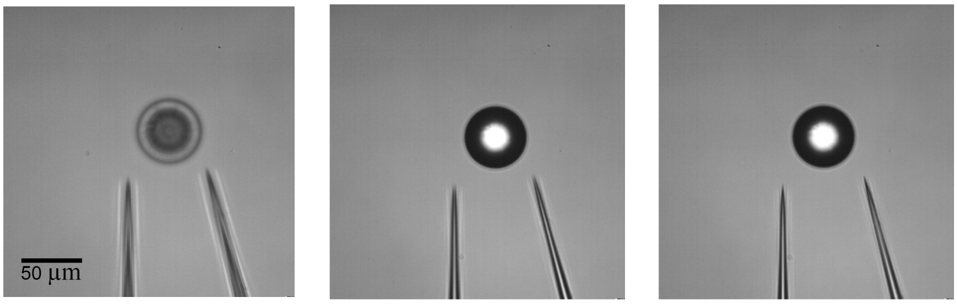

(a) (b) (c)

Figure 5.4: Autopositioning process: a) Initial situation (target object and end effectors are out of focus), b) After autofocusing to target object, c) After autopositioning end effectors.

New minimum search: In [82], termination criteria for minimum search were defined based on the observation of the relationship between the average intensity of the center region of the object, the average intensity of the stripe region, and the defocus function (Fig. 5.5). We noticed that previously defined termination criteria can cause a failure in object detection. Therefore, we simplified the minimum search and made the system more reliable. The procedure of the new minimum search is as follows:

- Find the crossing point where average intensity of center region is greater than that of stripe region (Fig. 5.5a), if not been found;
- When crossing point found, regard a point that has smaller value than its four neighbor points as a minimum candidate (Fig. 5.5c).

The flowchart of DFBIV after the modification is shown in Fig. 5.6. The process of DFBIV is will be:

0. Initialize camera, $k = 0, z = 89$
1. Capture frame number k from camera
2. Check if $k < 90$

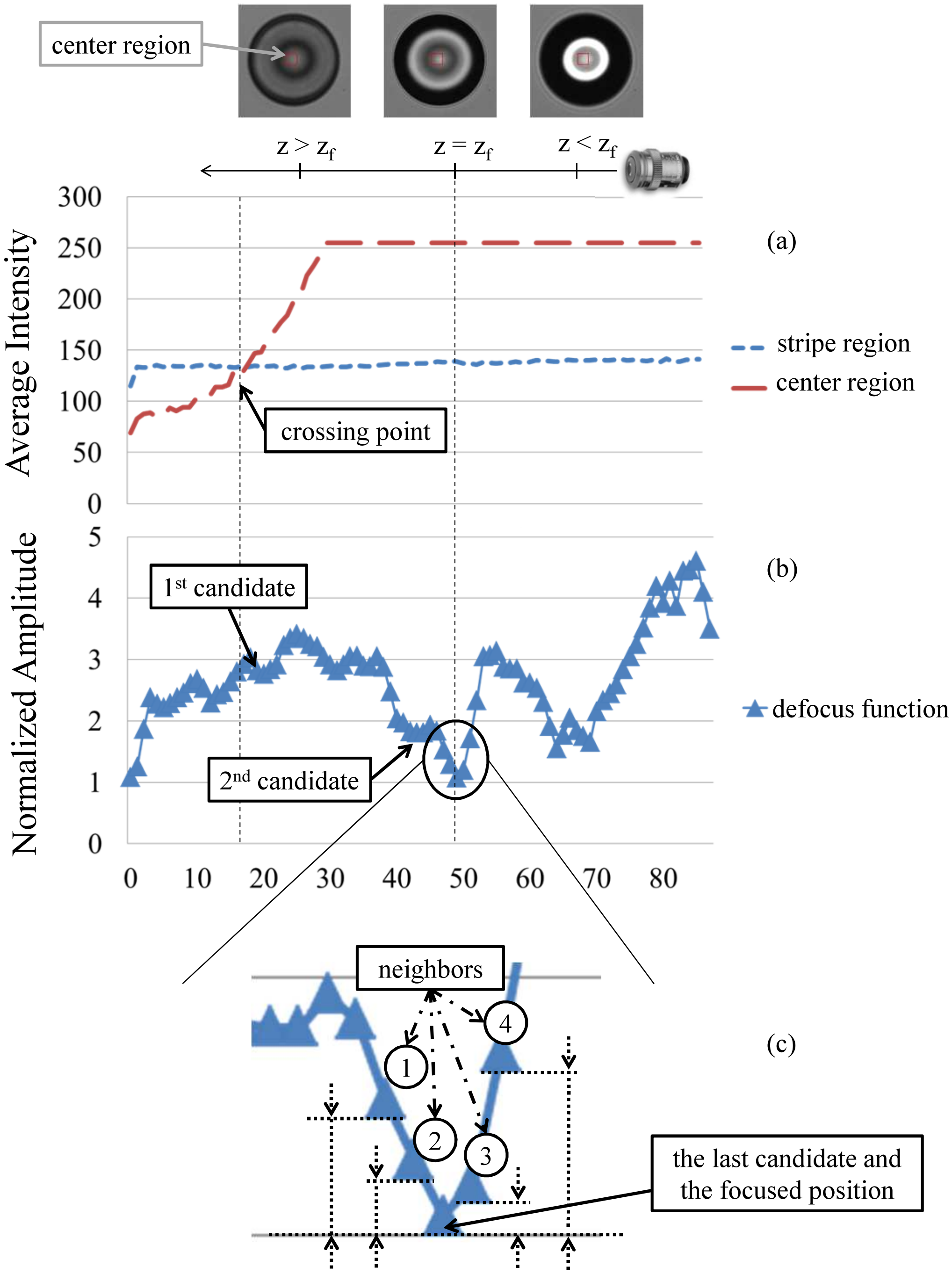

Figure 5.5: New minimum search.

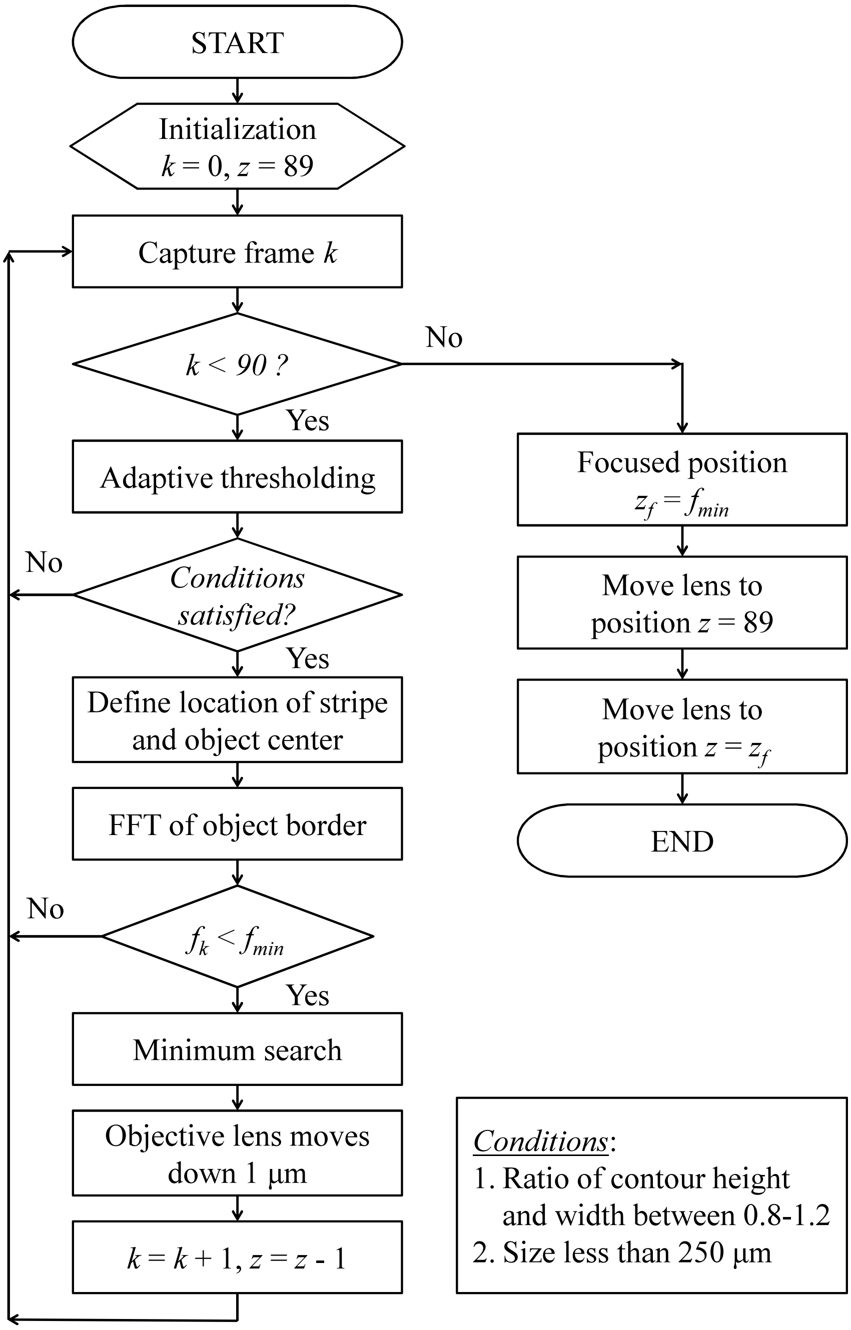
START
Initialization
$k = 0, z = 89$
Capture frame k
$k < 90$?
No
Yes
Adaptive thresholding
Conditions satisfied?
No
Yes
Define location of stripe and object center
FFT of object border
$f_k < f_{min}$
No
Yes
Minimum search
Objective lens moves down 1 µm
$k = k + 1, z = z - 1$
Focused position
$z_f = f_{min}$
Move lens to position $z = 89$
Move lens to position $z = z_f$
END
Conditions:
1. Ratio of contour height and width between 0.8-1.2
2. Size less than 250 µm

Figure 5.6: Flowchart of Depth From Border Intensity Variation.

3. Apply adaptive thresholding to captured frame k
4. Check the two conditions: ratio of found contour's height and width between 0.8 and 1.2, and size smaller than 250 μm, for round objects
5. Locate stripes and center of objects
6. Apply FFT to object border
7. Check only the case where $f_k < f_{min}$
8. Apply the new minimum search
9. Move lens down 1 μm, $k = k+1, z = z-1$
10. Continue steps 1-9 until $k = 90$
11. Regard the focused position $z_f = f_{min}$
12. Move lens to $z = 89$ then move lens to the focused position f_{min}

Autopositioning experiments have been carried out again after the modification of the detection algorithm. To check the robustness of the detection method, we tried to detect three different size microbeads (43-51-62 μm) and we altered the z-positions of targets by considering the range of the piezo actuator. Autopositioning process takes about 350 ms, with a success rate of 96% (96 out of 100 trials). We realized that failure cases were due to small quantities of dust in the microscopic field of view.

Zhang et al. achieved autopositioning through the detection of the contact between the end effector and the surface of the substrate within 5-8 sec. [57]. In this study, we propose a simpler and faster detection strategy –within 0.35 sec– for the target object and the end effector, by using the high-speed camera and the all-in-focus system.

5.2 Experimental Results and Discussion

As the ultimate goal is the pick-and-place of biological cells (size of 20–100 μm), manipulation of borosilicate microspheres (size of 40–60 μm) is performed in liquid. The fine stage is used for the positioning and transportation tasks where the parallel link mechanism is used for the grasping, releasing and vibration control tasks. Before a high-speed manipulation task performed, autofocusing to the target object and autopositioning of the end effectors carried out as explained in 5.1.2.2.

5.2.1 High-Speed Manipulation

After a successful autopositioning process, the system is ready for the manipulation task (Fig. 5.7). The most important part of high-speed micromanipulation is the accurate grasping of the object. The system detects the 2D position (x,y) of the end effectors and target object. As explained in related section (Vibration Compensation), the fine stage moves the end effectors to get close to the target at 2.3 mm/s. When the fine stage stops, the upper end effector starts to vibrate. The system applies feedforward control to compensate vibration. When the magnitude of the oscillation decreases to the imperceptible level, the parallel mechanism closes the upper end effector to grasp the object. The grasping distance for the upper end effector is decided with respect to the size of the target and space between the two fingers through visual feedback. After the grasping motion is completed, the high-speed grasping task is finished. The average duration of the high-speed grasping task is 290 ms, with a success rate of 100% (50 out of 50 trials). The high-speed grasping task is shown in Figs. 5.8a–c.

After grasping the target object firmly, the fine stage moves to a specific location (60 μm distance) with a speed of 2.3 mm/s. The success rate of the transportation task is 92% (46 out of 50 trials). The reason for the failures is the vibration of the end effector during the transportation motion. Finally, to release the target object, the parallel

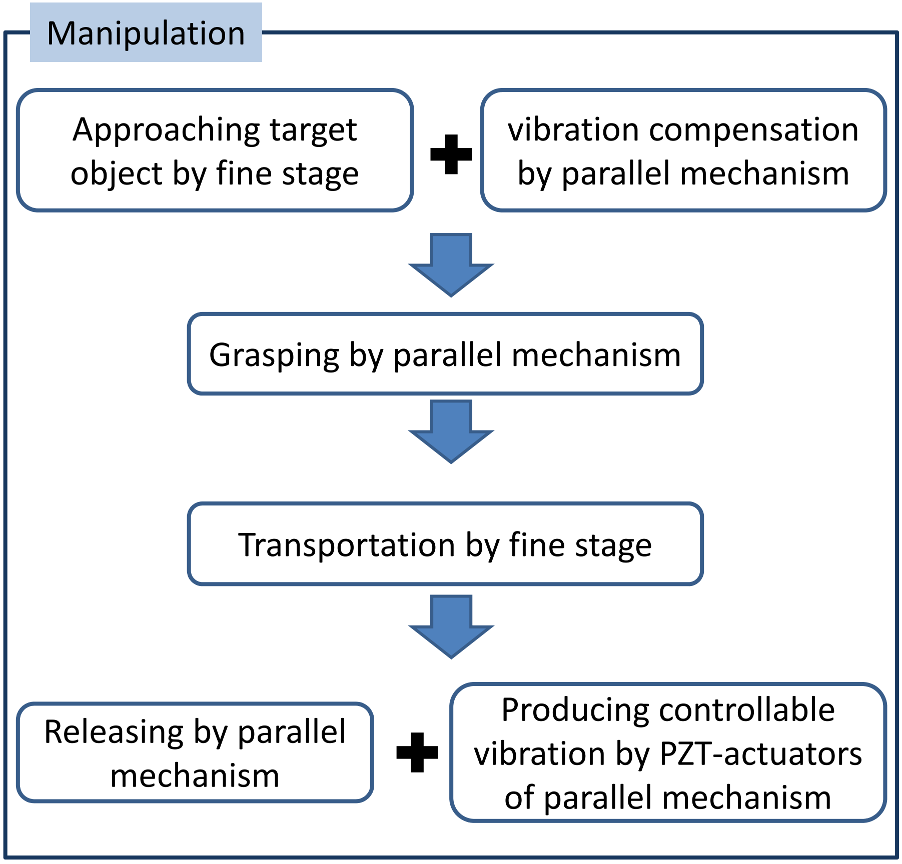
Manipulation
Approaching target object by fine stage
vibration compensation by parallel mechanism
Grasping by parallel mechanism
Transportation by fine stage
Releasing by parallel mechanism
Producing controllable vibration by PZT-actuators of parallel mechanism

Figure 5.7: Flow chart of high speed manipulation.

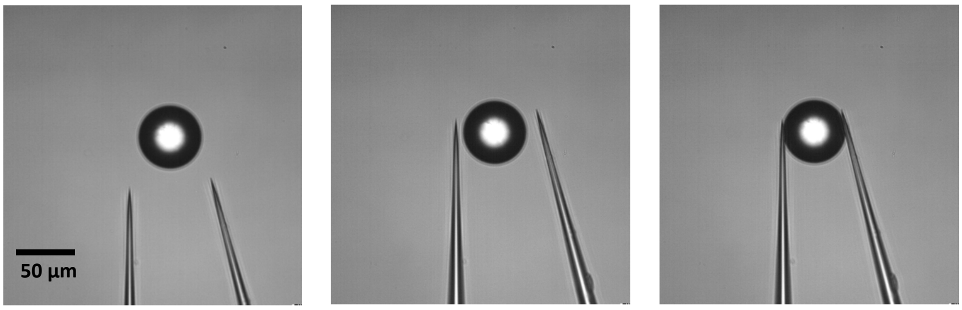

(a) (b) (c)

Figure 5.8: High-speed grasping: a) Ready to start manipulation task, b) After moving the end effectors to target object, c) After grasping target object.

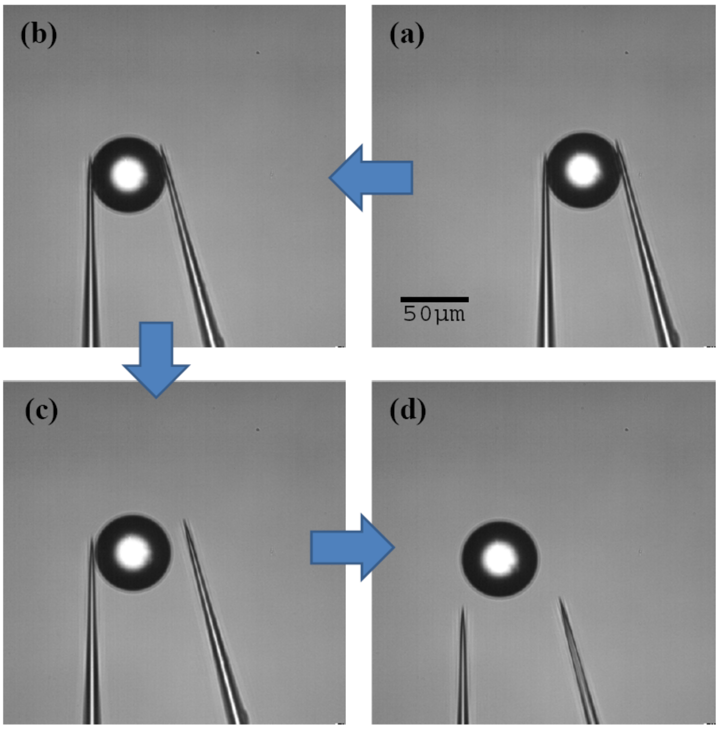

Figure 5.9: a) Ready for transportation, b) After transportation of target object, c) Releasing, d) End effectors moves away from target object.

mechanism opens the upper end effector; and the objects releases. However, sometimes, the target sticks the end effector due to adhesion forces. To achieve releasing of target object every time, piezo actuators of parallel mechanism generate vibration in the x-direction; and the fine stage moves both end effectors back. The success rate of the releasing task is 84% (42 out of 50 trials). The reason of the failures is attaching of the target objects to the left finger. The transportation and releasing tasks are completed in 670 ms, as shown in Fig. 5.9.

From the beginning of the grasping task to the end of the releasing task, the average duration is 960 ms. This manipulation time might change with respect to distance and speed. As an example to the high-speed application, 1D string of 3 microbeads has

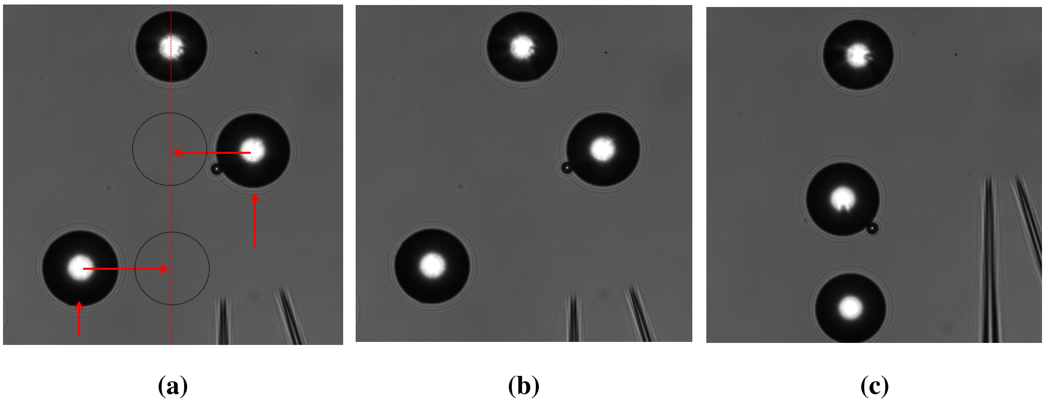
(a) (b) (c)

Figure 5.10: 1D microbeads string realization: a) Target positions, b) Before manipulation, c) After manipulation.

been achieved. However as target objects are in liquid environment, it is difficult to fix the objects to the specific position as seen in Fig. 5.10.

5.2.2 Discussion

The experimental results shows robustness of proposed 3D detection algorithm; and feasibility of manipulation of microobjects at high speed. To increase the manipulation success rate further, two parts can be improved. First, for the stable transportation of microobjects at high speed, oscillation during the motion should be reduced. Second, during the releasing task, for vibration generation, 3 directions (x-y-z) should be considered, not only the x-direction for finding optimum acceleration direction to overcome the adhesion forces which will be studied in our future work.

As explained above, during the experiments, failures might occur in two different situations. First, during the high-speed transportation task, the tightly held microobject may slip away due to vibration. In this case, system can find current position of the end effector and the target object to regrasp and complete the task. Second, during the releasing task, object might stick to the left finger which is fixed to fine stage and does not have relative motion ability. In this case, object should be detached from the end effector manually to continue to the experiments.

6

Conclusions

The system presented here allows single cell manipulation, including grasping, transporting, and releasing different-sized microobjects in the air and aqueous environments.

In the first part of the study, the micromanipulator was designed as a general-purpose microhand to replace task-specific systems, enabling us to use it in various microapplications. This general-purpose microhand can grasp multisized microobjects and transport them in a large workspace with precise positioning, which we call multi-scalability. To realize large workspace with precise motion for a transportation task, an automatic coarse-to-fine motion strategy based on visual servo-control has been realized. The visual feedback method developed for this study is a simple robust technique well-suited for micromanipulation systems. Currently, our system can transport microobjects of up to 25 mm with sub-micron precision. The system is compact enough for the microhand to be set up on an inverted microscope. Moreover, to realize large workspace for manipulating different-sized microobjects, the parallel link mechanism has also been optimized using inverse kinematics. we can currently manipulate microobjects of sizes between 1 and 132 μm, and a comparison with similar studies indicates the superiority of the proposed system.

In the second part of the study, manipulating microobjects automatically at high speed is carried out. We studied the residual vibration suppression in a microhand to achieve high-speed grasping of microobjects. First, we analyze the vibration behavior of both end effectors. Results show that for the speed of 2.3 mm/second, both end effectors' vibrations are great (29.1 μm and 5.76 μm max. deflections with $\approx$200 ms settling time) which is not appropriate for stable manipulation at high speed. To decrease the residual vibration of both end effectors, stiffness of the finger holders is increased. Consequently, the oscillation of the left end effector decreases to imperceptible level (1 μm with 20 ms settling time). However, the residual vibration of the right end effector is still great (25.88 μm with 173 ms settling time). To suppress the oscillation further, we implement the feedforward control. As a result, the amplitude of the vibration decreases by 47 % and the settling time decreases by 74 %. For this system, as we can predict the behavior of the vibration, the feedforward control method is suitable. To control the vibration due to any unexpected disturbance (vibrational motion of the microhand actuators on the platform due to imperfect design), feedback method can be applied. Thus, the combination of the feedforward and feedback methods would be a future work.

Moreover, a new fast detection algorithm to obtain the 3D positions of the end effector and the target microobject was developed. A top-down scanning of the target microobject and microfingers is performed by using a piezo actuator that can move the objective lens. And the information of the exact place of the center of the object and end effector is obtained. The system demonstrated that the pick-and-place of a borosilicate sphere can be performed in 1 second, which is faster than the highest speed reported in the literature thus far.

In our future work, we will concentrate on releasing task for the micromanipulation. As releasing of the target object is an ardous task in micro-scale, a robust method for the release will be the key factor for the high success rate pick-and-place task. Controllable vibration is one of the main methods to achieve releasing at high speed.

During the vibration generation, for the best result, three directions (x-y-z) of the end effector should be considered; not only the one direction to find the optimum acceleration direction to overcome the adhesion force.

References

[1] K. Inoue, T. Tanikawa, and T. Arai, “Micro-manipulation system with a two-fingered micro-hand and its potential application in bioscience,” *Journal of Biotechnology*, vol. 133, no. 2, pp. 219 – 224, 2008.

[2] “History of industrial robots,” http://www.ifr.org/history/, accessed: 05/31/2013.

[3] R. Fearing, “Survey of sticking effects for micro parts handling,” in *IEEE/RSJ International Conference on Intelligent Robots and Systems (IROS)*, vol. 2, 1995, pp. 212–217.

[4] A. Menciassi, A. Eisinberg, I. Izzo, and P. Dario, “From macro to micro manipulation: models and experiments,” *IEEE/ASME Transactions on Mechatronics*, vol. 9, no. 2, pp. 311–320, 2004.

[5] C.-N. Nguyen, “Vision-based 3d microsensing for automated micromanipulation,” *Ph.D. dissertation*, Osaka University, Osaka, 2012.

[6] M. Savia and H. Koivo, “Contact micromanipulation – survey of strategies,” *IEEE/ASME Transactions on Mechatronics*, vol. 14, no. 4, pp. 504–514, Aug. 2009.

[7] X. Wang, S. Chen, M. Kong, Z. Wang, K. D. Costa, R. A. Li, and D. Sun, “Enhanced cell sorting and manipulation with combined optical tweezer and microfluidic chip technologies,” *Lab Chip*, vol. 11, pp. 3656–3662, 2011.

[8] H. D. Ou-Yang and M.-T. Wei, “Complex fluids: Probing mechanical properties of biological systems with optical tweezers,” *Annual Review of Physical Chemistry*, vol. 61, no. 1, pp. 421–440, 2010.

[9] A. Banerjee, A. Pomerance, W. Losert, and S. Gupta, “Developing a stochastic dynamic programming framework for optical tweezer-based automated particle transport operations,” *IEEE Transactions on Automation Science and Engineering*, vol. 7, no. 2, pp. 218–227, 2010.

[10] M. Kharboutly, M. Gauthier, and N. Chaillet, “Modeling the trajectory of a micro particle in a dielectrophoresis device for dynamic control,” in *IEEE International Conference on Robotics and Automation (ICRA)*, 2010, pp. 4125–4130.

[11] H. Maruyama, K. Kotani, T. Masuda, A. Honda, T. Takahata, and F. Arai, “Nanomanipulation of single influenza virus using dielectrophoretic concentration and optical tweezers for single virus infection to a specific cell on a microfluidic chip,” *Microfluidics and Nanofluidics*, vol. 10, no. 5, pp. 1109–1117, 2011.

[12] W. Liang, S. Wang, Z. Dong, G.-B. Lee, and W. J. Li, “Optical spectrum and electric field waveform dependent optically-induced dielectrophoretic (odep) micro-manipulation,” *Micromachines*, vol. 3, no. 2, pp. 492–508, 2012.

[13] T. Masuda, M. Niimi, H. Nakanishi, Y. Yamanishi, and F. Arai, “Cancer cell separator using size-dependent filtration in microfluidic chip,” *Sensors and Actuators B: Chemical*, vol. 185, no. 0, pp. 245 – 251, 2013.

[14] A. Haake, A. Neild, D.-H. Kim, J.-E. Ihm, Y. Sun, J. Dual, and B.-K. Ju, “Manipulation of cells using an ultrasonic pressure field,” *Ultrasound in Medicine & Biology*, vol. 31, no. 6, pp. 857–864, 2005.

[15] J. Hultström, O. Manneberg, K. Dopf, H. Hertz, H. Brismar, and M. Wiklund, “Proliferation and viability of adherent cells manipulated by standing-wave ultrasound in a microfluidic chip,” *Ultrasound in Medicine & Biology*, vol. 33, no. 1, pp. 145–151, 2007.

[16] T. Laurell, F. Petersson, and A. Nilsson, “Chip integrated strategies for acoustic separation and manipulation of cells and particles,” *Chemical Society Review*, vol. 36, pp. 492–506, 2007.

[17] G. Thalhammer, R. Steiger, M. Meinschad, M. Hill, S. Bernet, and M. Ritsch-Marte, "Combined acoustic and optical trapping," *Biomedical Optics Express*, vol. 2, no. 10, pp. 2859–2870, Oct. 2011.

[18] S. Arumuganathar, S. Irvine, J. McEwan, and S. Jayasinghe, "Aerodynamically assisted bio-jets: The development of a novel and direct non-electric field-driven methodology for engineering living organisms," *Biomedical Materials*, vol. 2, no. 2, pp. 158–168, May 2007.

[19] E. Griessinger, S. Jayasinghe, and D. Bonnet, "Aerodynamically assisted bio-jetting of hematopoietic stem cells," *The Analyst*, vol. 137, no. 6, pp. 1329–1333, Feb. 2012.

[20] T. Tanikawa and T. Arai, "Development of a micro-manipulation system having a two-fingered micro-hand," *IEEE Transactions on Robotics and Automation*, vol. 15, no. 1, pp. 152–162, 1999.

[21] Y. Yamanishi, S. Sakuma, K. Onda, and F. Arai, "Biocompatible polymeric magnetically driven microtool for particle sorting," *Journal of Micro - Nano Mechatronics*, vol. 4, no. 1, pp. 49–57, 2008.

[22] Y. Yamanishi, S. Sakuma, Y. Kihara, and F. Arai, "Fabrication and application of 3-d magnetically driven microtools," *Journal of Microelectromechanical Systems*, vol. 19, no. 2, pp. 350–356, April 2010.

[23] Y. Yamanishi, T. Mizunuma, N. Inomata, S. Kudo, and F. Arai, "Soft scrubbing off of zona pellucida on disposable microfluidic chip," in *IEEE 23rd International Conference on Micro Electro Mechanical Systems*, Jan. 2010, pp. 256–259.

[24] F. Arai, N. Inomata, S. Kudo, Y. Yamanishi, and T. Mizunuma, "Omni-directional actuation of magnetically driven microtool for enucleation of oocyte," in *IEEE 23rd International Conference on Micro Electro Mechanical Systems*, Jan. 2010, pp. 1167–1170.

[25] A. Ichikawa, S. Takahashi, K. Matsukawa, T. Tanikawa, and K. Ohba, “Injection and cutting methods of animal cells using a microfluidic chip,” in *IEEE International Conference on Robotics and Automation*, May 2008, pp. 868–873.

[26] Y. Yamanishi, S. Sakuma, T. Iyanagi, F. Arai, T. Arai, A. Hasegawa, T. Tanikawa, A. Ichikawa, O. Satoh, A. Nakayama, H. Aso, M. Goto, S. Takahashi, and K. Matsukawa, “Design and fabrication of all-in-one unified microfluidic chip for automation of embryonic cell manipulation,” *Journal of Robotics and Mechatronics*, vol. 22, no. 3, pp. 371–379, 2010.

[27] H. Xie and R. S., “Three-dimensional automated micromanipulation using a nanotip gripper with multi-feedback,” *Journal of Micromechanics and Microengineering*, vol. 19, no. 7, p. 075009, 2009.

[28] B. Chen, Y. Zhang, and Y. Sun, “Active release of microobjects using a mems microgripper to overcome adhesion forces,” *Journal of Microelectromechanical Systems*, vol. 18, no. 3, pp. 652–659, June 2009.

[29] Z. Lu, C. Moraes, Y. Zhao, L. You, C. Simmons, and Y. Sun, “A micromanipulation system for single cell deposition,” in *IEEE International Conference on Robotics and Automation*, May 2010, pp. 494–499.

[30] Z. Lu, X. Zhang, C. Leung, N. Esfandiari, R. Casper, and Y. Sun, “Robotic icsi (intracytoplasmic sperm injection),” *IEEE Transactions on Biomedical Engineering*, vol. 58, no. 7, pp. 2102–2108, July 2011.

[31] M. Takeuchi, M. Nakajima, M. Kojima, and T. Fukuda, “Evaluation and application of thermoresponsive gel handling towards manipulation of single cells,” in *IEEE/RSJ International Conference on Intelligent Robots and Systems*, Sept. 2011, pp. 457–462.

[32] C. Nguyen, K. Ohara, E. Avci, T. Takubo, Y. Mae, and T. Arai, “Automated micromanipulation for a microhand with all-in-focus imaging system,” in *IEEE/RSJ International Conference on Intelligent Robots and Systems*, Sept. 2011, pp. 427–432.

[33] E. Avci, K. Ohara, T. Takubo, Y. Mae, and T. Arai, “A new multi-scale micromanipulation system with dexterous motion,” in *International Symposium of Micro-NanoMechatronics and Human Science*, 2009, pp. 444–449.

[34] N. Dechev, J. K. Mills, and W. L. Cleghorn, “Mechanical fastener designs for use in the microassembly of 3d microstructures,” in *Proceedings of the ASME International Mechanical Engineering Congress and RD&D Expo*, 2004, pp. 13–19.

[35] A. Das, R. Murthy, D. Popa, and H. Stephanou, “A multiscale assembly and packaging system for manufacturing of complex micro-nano devices,” *IEEE Transactions on Automation Science and Engineering*, vol. 9, no. 1, pp. 160–170, 2012.

[36] C. Clvy, A. Hubert, and N. Chaillet, “Flexible micro-assembly system equipped with an automated tool changer,” *Journal of Micro-Nano Mechatronics*, vol. 4, no. 1-2, pp. 59–72, 2008.

[37] B. Tamadazte, N. Le Fort-Piat, S. Dembele, and E. Marchand, “Microassembly of complex and solid 3d mems by 3d vision-based control,” in *IEEE/RSJ International Conference on Intelligent Robots and Systems (IROS)*, 2009, pp. 3284–3289.

[38] M. Gauthier, E. Gibeau, and D. Heriban, “Submerged robotic micromanipulation and dielectrophoretic micro-object release,” in *9th International Conference on Control, Automation, Robotics and Vision (ICARCV ’06)*, 2006, pp. 1–6.

[39] A. Bolopion, H. Xie, D. Haliyo, and S. Regnier, “3d haptic handling of microspheres,” in *IEEE/RSJ International Conference on Intelligent Robots and Systems (IROS)*, 2010, pp. 6131–6136.

[40] H. Xie, J. C. Acosta, and S. Regnier, “Achieving three-dimensional automated micromanipulation at the scale of several micrometers with a nanotip gripper,” in *IEEE/RSJ International Conference on Intelligent Robots and Systems (IROS)*, 2009, pp. 761–766.

[41] T. Chen, L. Chen, L. Sun, W. Rong, and Q. Yang, "Micro manipulation based on adhesion control with compound vibration," in *IEEE/RSJ International Conference on Intelligent Robots and Systems (IROS)*, 2010, pp. 6137–6142.

[42] K. Kawashima, T. Arai, K. Tadano, T. Fujita, and T. Kagawa, "Development of coarse/fine dual stage using pneumatically driven bellows actuator and cylinder with air bearings," *Precision Engineering*, vol. 34, no. 3, pp. 526 – 533, 2010.

[43] L. Ren, L. Wang, J. Mills, and D. Sun, "Vision-based 2-d automatic micrograsping using coarse-to-fine grasping strategy," *IEEE Transactions on Industrial Electronics*, vol. 55, no. 9, pp. 3324–3331, 2008.

[44] C. Mason, P. Dunnill *et al.*, "A brief definition of regenerative medicine," *Regenerative medicine*, vol. 3, no. 1, pp. 1–6, 2008.

[45] J. Yang, M. Yamato, C. Kohno, A. Nishimoto, H. Sekine, F. Fukai, and T. Okano, "Cell sheet engineering: recreating tissues without biodegradable scaffolds," *Biomaterials*, vol. 26, no. 33, pp. 6415–6422, 2005.

[46] C. Norotte, F. S. Marga, L. E. Niklason, and G. Forgacs, "Scaffold-free vascular tissue engineering using bioprinting," *Biomaterials*, vol. 30, no. 30, pp. 5910–5917, 2009.

[47] M. Nakamura, S. Iwanaga, K. Arai, H. Toda, G. Capi, and T. Nikaido, "Computer-assisted biofabrication: The challenges on manufacturing 3-d biological tissues for tissue and organ engineering," in *Symposium on VLSI Technology (VLSIT)*, 2011, pp. 2–5.

[48] J. A. Thompson and R. Fearing, "Automating microassembly with ortho-tweezers and force sensing," in *IEEE/RSJ International Conference on Intelligent Robots and Systems*, vol. 3, 2001, pp. 1327–1334.

[49] G. Yang, J. A. Gaines, and B. J. Nelson, "A supervisory wafer-level 3d microassembly system for hybrid mems fabrication," *J. Intell. Robotics Syst.*, vol. 37, no. 1, pp. 43–68, 2003.

[50] N. Dechev, W. Cleghorn, and J. Mills, "Microassembly of 3-d microstructures using a compliant, passive microgripper," *Journal of Microelectromechanical Systems*, vol. 13, no. 2, pp. 176–189, 2004.

[51] A. Ferreira, C. Cassier, and S. Hirai, "Automatic microassembly system assisted by vision servoing and virtual reality," *IEEE/ASME Transactions on Mechatronics*, vol. 9, no. 2, pp. 321–333, 2004.

[52] K. Tsui, A. A. Geisberger, M. Ellis, and G. D. Skidmore, "Micromachined end-effector and techniques for directed mems assembly," *Journal of Micromechanics and Microengineering*, vol. 14, no. 4, p. 542, 2004.

[53] A. Hoover and R. Fearing, "Rapidly prototyped orthotweezers for automated microassembly," in *IEEE International Conference on Robotics and Automation*, 2007, pp. 812–819.

[54] C. Onal and M. Sitti, "Visual servoing-based autonomous 2-d manipulation of microparticles using a nanoprobe," *IEEE Transactions on Control Systems Technology*, vol. 15, no. 5, pp. 842–852, 2007.

[55] D. Heriban and M. Gauthier, "Robotic micro-assembly of microparts using a piezogripper," in *IEEE/RSJ International Conference on Intelligent Robots and Systems (IROS)*, 2008, pp. 4042–4047.

[56] C.-N. Nguyen, K. Ohara, E. Avci, T. Takubo, Y. Mae, and T. Arai, "Real-time precise 3d measurement of micro transparent objects using all-in-focus imaging system," *Journal of Micro-Nano Mechatronics*, vol. 7, no. 1-3, pp. 21–31, 2012.

[57] Y. Zhang, B. Chen, X. Liu, and Y. Sun, "Autonomous robotic pick-and-place of microobjects," *IEEE Transactions on Robotics*, vol. 26, no. 1, pp. 200–207, 2010.

[58] K. Inoue, D. Nishi, T. Takubo, and T. Arai, "Measurement of mechanical properties of living cells using micro fingers and afm cantilevers," in *International Symposium on Micro-NanoMechatronics and Human Science*, 2006, pp. 1–6.

[59] D. Kawakami, K. Ohara, T. Takubo, Y. Mae, A. Ichikawa, T. Tanikawa, and T. Arai, “Cell stiffness measurement using two-fingered microhand,” in *IEEE International Conference on Robotics and Biomimetics (ROBIO)*, 2010, pp. 1019–1024.

[60] P. R. Ouyang, R. C. Tjiptoprodjo, W. J. Zhang, and G. S. Yang, “Micro-motion devices technology: The state of arts review,” *The International Journal of Advanced Manufacturing Technology*, vol. 38, no. 5-6, pp. 463–478, 2008.

[61] A. Ramadan, T. Takubo, Y. Mae, K. Oohara, and T. Arai, “Developmental process of a chopstick-like hybrid-structure two-fingered micromanipulator hand for 3-d manipulation of microscopic objects,” *IEEE Transactions on Industrial Electronics*, vol. 56, no. 4, pp. 1121–1135, 2009.

[62] E. Avci, K. Ohara, T. Takubo, Y. Mae, and T. Arai, “High speed micromanipulation system with multi-scalability,” in *IEEE International Conference on Robotics and Biomimetics (ROBIO)*, 2011, pp. 1212–1217.

[63] J.-P. Merlet, *Parallel robots*. Springer, 2006.

[64] W. Tao, M. Zhang, M. Liu, and X. Yun, “Residual vibration analysis and suppression for scara robot arm in semiconductor manufacturing,” in *IEEE/RSJ International Conference on Intelligent Robots and Systems (IROS)*, 2006, pp. 5153–5158.

[65] T. Chang and X. Sun, “Analysis and control of monolithic piezoelectric nano-actuator,” *IEEE Transactions on Control Systems Technology*, vol. 9, no. 1, pp. 69–75, 2001.

[66] M. Rakotondrabe, C. Clevy, and P. Lutz, “Hysteresis and vibration compensation in a nonlinear unimorph piezocantilever,” in *IEEE/RSJ International Conference on Intelligent Robots and Systems (IROS)*, 2008, pp. 558–563.

[67] M. Rakatondrabe, C. Clevy, and P. Lutz, “Complete open loop control of hysteretic, creeped, and oscillating piezoelectric cantilevers,” *IEEE Transactions on Automation Science and Engineering*, vol. 7, no. 3, pp. 440–450, 2010.

[68] M. Rakotondrabe, K. Rabenorosoa, J. Agnus, and N. Chaillet, “Robust feedforward-feedback control of a nonlinear and oscillating 2-dof piezocantilever,” *IEEE Transactions on Automation Science and Engineering*, vol. 8, no. 3, pp. 506–519, 2011.

[69] K. Inoue, D. Nishi, T. Takubo, T. Tanikawa, and T. Arai, “Performance evaluation of teleoperation for manipulating micro objects using two-fingered micro hand,” *Journal of Robotics and Mechatronics*, vol. 19, no. 5, pp. 577–584, 2007.

[70] J. Roy and L. L. Whitcomb, “Comparative structural analysis of 2-dof semi-direct-drive linkages for robot arms,” *IEEE/ASME Transactions on Mechatronics*, vol. 4, no. 1, pp. 82–86, 1999.

[71] N. Y. Kim and M. S. Hong, “Diagnosis and reduction of robot arm vibration for 12-inch wafer spin scrubber,” *Key Engineering Materials*, vol. 270, pp. 884–889, 2004.

[72] P. Lambrechts, M. Boerlage, and M. Steinbuch, “Trajectory planning and feedforward design for high performance motion systems,” in *American Control Conference*, vol. 5, 2004, pp. 4637–4642.

[73] P. H. Meckl and P. B. Arestides, “Optimized s-curve motion profiles for minimum residual vibration,” in *American Control Conference*, vol. 5, 1998, pp. 2627–2631.

[74] A. Abe and K. Komuro, “Minimum energy trajectory planning for vibration control of a flexible manipulator using a multi-objective optimisation approach,” *Int. J. of Mechatronics and Automation*, vol. 2, no. 4, pp. 286–294, 2012.

[75] T. Singh and W. Singhose, “Input shaping/time delay control of maneuvering flexible structures,” in *American Control Conference*, vol. 3, 2002, pp. 1717–1731.

[76] W. E. Singhose and N. C. Singer, “Effects of input shaping on two-dimensional trajectory following,” *IEEE Transactions on Robotics and Automation*, vol. 12, no. 6, pp. 881–887, 1996.

[77] A. Piazzi and A. Visioli, “Minimum-time system-inversion-based motion planning for residual vibration reduction,” *IEEE/ASME Transactions on Mechatronics*, vol. 5, no. 1, pp. 12–22, 2000.

[78] M. McEver and D. J. Leo, “Autonomous vibration suppression using on-line pole-zero identification,” *J. Vib. Acoust*, vol. 123, no. 4, pp. 487–495, 2001.

[79] A. Preumont, A. François, F. Bossens, and A. Abu-Hanieh, “Force feedback versus acceleration feedback in active vibration isolation,” *Journal of Sound and Vibration*, vol. 257, no. 4, pp. 605–613, 2002.

[80] E. Avci, C.-N. Nguyen, K. Ohara, Y. Mae, T. Arai, and C. Gobel, “Vibration analysis of microhand for high speed single cell manipulation,” in *International Conference on Mechatronics and Automation (ICMA)*, 2012, pp. 75–80.

[81] C.-N. Nguyen, K. Ohara, T. Takubo, Y. Mae, and T. Arai, “High-speed autofocusing of multisized microobjects,” in *IEEE International Conference on Automation Science and Engineering (CASE)*, 2012, pp. 34–39.

[82] E. Avci, C.-N. Nguyen, K. Ohara, M. Kojima, Y. Mae, and T. Arai, “Towards high-speed automated micromanipulation,” in *IEEE International Conference on Robotics and Automation*, 2013, pp. 1710–1715.

Publications

Journals

1. [Under review] **Ebubekir AVCI**, Kenichi Ohara, Chayooth Theeravithayangkura, Chanh-Nghiem Nguyen, Masaru Kojima, Yasushi Mae, and Tatsuo Arai, “High-Speed Automated Manipulation of Microobjects Using Two-Fingered Microhand,” *IEEE Transactions on Industrial Electronics*.

2. **Ebubekir AVCI**, Chanh-Nghiem Nguyen, Kenichi Ohara, Yasushi Mae, and Tatsuo Arai, “Analysis and Suppression of Residual Vibration in Microhand for High-Speed Single-Cell Manipulation,” *International Journal of Mechatronics and Automation*, Vol. 3, No. 2, pp. 110-117, 2013.

3. **Ebubekir AVCI**, Kenichi Ohara, Tomohito Takubo, Yasushi Mae, and Tatsuo Arai, “Development of Multi-Scalable Microhand System with Precise Motion,” *Journal of Robotics and Mechatronics*, Vol. 25, No. 1, pp. 183-191, 2013.

4. Chanh-Nghiem Nguyen, Kenichi Ohara, **Ebubekir AVCI**, Tomohito Takubo, Yasushi Mae, and Tatsuo Arai, “Real-time Precise 3D Measurement of Micro Transparent Objects Using All-In-Focus Imaging System,” *Journal of Micro-Nano Mechatronics*, Vol. 7, pp. 21-31, 2012.

International conferences

1. **Ebubekir Avci**, Chanh-Nghiem Nguyen, Kenichi Ohara, Masaru Kojima, Yasushi Mae, Tatsuo Arai, "Towards High Speed Automated Micromanipulation," *in IEEE International Conference on Robotics and Automation*, Karlsruhe, Germany, May 6-10, 2013, pp. 1710–1715.

2. **Ebubekir Avci**, Kenichi Ohara, Tatsuo Arai, "Towards High-Speed Microassembly Using Two-fingered Microhand," *in ICRA 2013 Workshop: Microassembly: Robotics and Beyond*, Karlsruhe, Germany, May 6-10, 2013, pp. 11–12.

3. Masaru Kojima, **Ebubekir Avci**, Kenichi Ohara, Yasushi Mae, Tatsuo Arai, "Development of End Effector for Cell Manipulation with Two-fingered Microhand," *in 23rd IEEE International Symposium on Micro-Nano Mechatronics and Human Science*, Nagoya, Japan, Nov.4-7, 2012, pp.399–401.

4. **Ebubekir Avci**, Christoph Gobel, Chanh-Nghiem Nguyen, Kenichi Ohara, Yasushi Mae, and Tatsuo Arai, "Vibration Analysis of Microhand for High Speed Single Cell Manipulation," *in IEEE International Conference on Mechatronics and Automation*, Chengdu, China, Aug. 5–8, 2012, pp. 75–80.

5. **Ebubekir Avci**, Kenichi Ohara, Tomohito Takubo, Yasushi Mae, Tatsuo Arai, "High Speed Micromanipulation System with Multi-Scalability," *in IEEE International Conference on Robotics and Biomimetics*, Phuket, Thailand, Dec. 7-11, 2011, pp.1212–1217. **Finalist of T. J. Tarn Best Paper in Robotics**

6. Chanh-Nghiem Nguyen, Kenichi Ohara, **Ebubekir Avci**, Tomohito Takubo, Yasushi Mae, and Tatsuo Arai, "Automated Micromanipulation of a Microhand

with All-In-Focus Imaging System," *in IEEE/RSJ International Conference on Intelligent Robots and Systems*, San Francisco, USA, Sept. 25–30, 2011, pp. 427–432.

7. **Ebubekir Avci**, Kenichi Ohara, Tomohito Takubo, Yasushi Mae, Tatsuo Arai, "Workspace Optimization for Multi-Scale Micromanipulation System," *in 21st IEEE International Symposium on Micro-Nano Mechatronics and Human Science*, Nov.7-10, 2010, pp.328–333.

8. **Ebubekir Avci**, Kenichi Ohara, Tomohito Takubo, Yasushi Mae, Tatsuo Arai, "A new Multi-Scale Micromanipulation System with Dexterous Motion," *in 20th IEEE International Symposium on Micro-Nano Mechatronics and Human Science*, Nagoya, Japan, November 8-11, 2009, pp. 444–449.

Domestic conferences

1. Chanh-Nghiem Nguyen, Kenichi Ohara, **Ebubekir Avci**, Tomohito Takubo, Yasushi Mae, and Tatsuo Arai, "High-Speed 3D Detection and Tracking of a Two-Fingered Microhand," *in SICE 2011 Annual Conference*, pp. 2K2_3, Kyoto, Japan, Dec. 23–25, 2011.

2. **Ebubekir Avci**, Kenichi Ohara, Tomohito Takubo, Yasushi Mae, Tatsuo Arai, "Optimum Design for Multi-Scalable Microhand," *in 28th Annual Conference of the Robotics Society of Japan*, Nagoya, Japan, September 22-24, 2010, pp. 3M1_5.

3. **Ebubekir Avci**, Kenichi Ohara, Tomohito Takubo, Yasushi Mae, Tatsuo Arai, "A new Multi-Scale Micromanipulation System," *in 27th Annual Conference of*

the Robotics Society of Japan, Yokohama, Japan, September 15-17, 2009, pp. 1B1_02.